# UNIVERSAL PHOTOLUMINESCENCE ENHANCEMENT/SUPPRESSION AT THE VERTICAL VAN DER WAALS METAL-SEMICONDUCTOR INTERFACES

A THESIS SUBMITTED TO

THE GRADUATE SCHOOL OF ENGINEERING AND SCIENCE

OF BILKENT UNIVERSITY

IN PARTIAL FULFILLMENT OF THE REQUIREMENTS FOR

THE DEGREE OF

MASTER OF SCIENCE

IN

PHYSICS

By

Hafiz Muhammad Shakir

January 2024

Universal photoluminescence enhancement/suppression at the vertical van der Waals metal-semiconductor interfaces
By Hafiz Muhammad Shakir
January 2024

We certify that we have read this thesis and that in our opinion it is fully adequate, in scope and in quality, as a thesis for the degree of Master of Science.

Talip Serkan Kasirga(Advisor)

Alpan Bek

Ibrahim Sarpkaya

Approved for the Graduate School of Engineering and Science:

Orhan Arikan
Director of the Graduate School

# ABSTRACT

# UNIVERSAL PHOTOLUMINESCENCE ENHANCEMENT/SUPPRESSION AT THE VERTICAL VAN DER WAALS METAL-SEMICONDUCTOR INTERFACES

Hafiz Muhammad Shakir
M.S. in Physics
Advisor: Talip Serkan Kasirga
January 2024

Monolayers of transition metal dichalcogenides are considered the prospects for optoelectronic devices and photoluminescence (PL) is one of the key parameters to observe the performance and efficiency of such devices. The PL characteristics of monolayers of semiconducting transition metal dichalcogenides (TMDCs) have been consistently reported to be suppressed in the presence of metal, a phenomenon observed through direct metal evaporation or annealing of heterostructures in prior studies. These methods often resulted in a significant negative charge transfer which creates metal-induced gap states (MIGS) and Fermi level pinning (FLP). These MIGS and FLP provide nonradiative pathways to the excited electrons causing a huge suppression in PL intensity.

To address this challenge, we explore heterostructures with a van der Waals gap between the metal and semiconductor surfaces. This design reduces the nonradiative relaxation pathways, allowing for more controlled charge transfer due to the van der Waals gap and the modulation of Schottky barrier height (SBH). The SBH for electrons increases with increasing metal work function and hence provides direct control of charge injection type and magnitude to monolayers of TMDCs.

Our research presents a universal methodology for controlling the PL intensity of TMDCs by strategically utilizing the van der Waals gap and tailoring the work function of the interfacing metal. This investigation not only unveils a novel approach to prevent PL quenching but also opens avenues for optimizing optoelectronic devices. By carefully selecting metallic and semiconducting materials,

this work offers a pathway to enhance device performance and precisely regulate output characteristics in optoelectronic applications.

*Keywords:* Photoluminescence, transition metal dichalcogenides, van der Waals gap, Schottky barrier height, and optoelectronics.

# ÖZET

# DIKEY VAN DER WAALS METAL-YARI ILETKEN ARAYÜZLERINDE EVRENSEL FOTOLÜMINESANS GELIŞTIRME/BASTRMA

Hafiz Muhammad Shakir
fizik Mühendisliği, Yüksek Lisans
Tez Danışmanı: Talip Serkan Kasirga
Ocak 2024

Geçiş metali dikalkojenitlerin tek katmanları, optoelektronik cihazlar için potansiyel olarak kabul edilir ve fotolüminesans (PL), bu tür cihazların performansını ve verimliliğini gözlemlemek için temel parametrelerden biridir. Yarı iletken geçiş metali dikalkojenitlerin (TMDC'ler) tek katmanlarının PL özelliklerinin, önceki çalışmalarda doğrudan metal buharlaşması veya heteroyapıların tavlanması yoluyla gözlemlenen bir fenomen olan metal varlığında sürekli olarak bastırıldığı rapor edilmiştir. Bu yöntemler genellikle metal kaynaklı boşluk durumları (MIGS) ve Fermi düzeyinde sabitleme (FLP) oluşturan önemli bir negatif yük aktarımıyla sonuçlandı. Bu MIGS ve FLP, uyarılmış elektronlara ışınımsız yollar sağlayarak PL yoğunluğunda büyük bir baskılamaya neden olur.

Bu zorluğun üstesinden gelmek için metal ve yarı iletken yüzeyler arasında van der Waals boşluğu bulunan heteroyapıları araştırıyoruz. Bu tasarım, ışınımsal olmayan gevşeme yollarını azaltarak van der Waals boşluğu ve Schottky bariyer yüksekliğinin (SBH) modülasyonu nedeniyle daha kontrollü yük aktarımına olanak tanır. Elektronlar için SBH, artan metal iş fonksiyonuyla birlikte artar ve dolayısıyla TMDC'lerin tek katmanlarına yük enjeksiyon tipinin ve büyüklüğünün doğrudan kontrolünü sağlar.

Araştırmamız, van der Waals boşluğunu stratejik olarak kullanarak ve arayüz oluşturan metalin iş fonksiyonunu uyarlayarak TMDC'lerin PL yoğunluğunu kontrol etmek için evrensel bir metodoloji sunmaktadır. Bu araştırma sadece PL sönümlemesini önlemek için yeni bir yaklaşımı ortaya çıkarmakla kalmıyor, aynı zamanda optoelektronik cihazların optimize edilmesi için yollar da açıyor. Metalik ve yarı iletken malzemeleri dikkatle seçerek bu çalışma, optoelektronik uygulamalarda cihaz performansını artırmaya ve çıkış özelliklerini hassas bir şekilde

düzenlemeye yönelik bir yol sunuyor.

*Anahtar sözcükler*: Anahtar Sözlerim.

# Acknowledgement

I am extremely grateful to Prof. Talip Serkan Kasirga for accepting me as a research student in his esteemed group and allowing me to begin my new journey in the field of experimental condensed matter physics. I have always admired his approach and critical thinking towards science and have tried to adopt the same approach. He not only guided me throughout the last two years to learn and complete my thesis but also supported me through all the ups and downs. He is not only a great scientist but also a wonderful human being. He shared his personal life experiences with me for motivation and guided me in every step of my research project. I am truly thankful for his mentorship and guidance.

I am immensely grateful to Prof. Alpan Bek from METU and Prof. Ibrahim Sarpakaya from UNAM-Bilkent for accepting our invitation and taking out time from their busy schedules to serve as jury members. I extend my heartfelt thanks to Alpan Hoca for adjusting his schedule to accommodate our time constraints for this defense. I am also thankful to Ibrahim Hoca and his team members, Atif Dormus and Hilal Korkut, for their collaboration on my project and for conducting low-temperature measurements multiple times.

I would like to express my gratitude towards Dr. Abdulsalam Aji Suleiman for his unwavering guidance and support throughout my research journey. He is not only a senior and a fellow member of our group but also an elder brother figure who has patiently taught me every minute detail of research life. I am also highly thankful to my current and previous SCMLab members, including Muhammad Ali Razeghi, Amir Parsi, Ugur Basci, Oughzhan Ougz, Doruk Pehlivanoglu, Engin Can Surmeli, and Onur Alp. They have created a peaceful and friendly learning environment that has helped me learn a lot of new things. I am grateful for their assistance.

I would like to express my heartfelt gratitude to my family members, especially my parents, who have always supported me throughout my journey and extended their cooperation whenever needed. I am immensely grateful to my wonderful and

patient wife who has stood by my side and compromised at every single moment of our married life. I would also like to pay my special regards to my brothers and their wives, and sisters who have always been there to support me, my wife, and my kids, and have helped keep the whole family together.

I have a Bilkent Family as well who welcomed me from the very first day of joining Bilkent. First of all, I would like to especially thank my dearest friend Mohsin Waris who always supported me and pushed me to start my career as a Bilkent member. After Mohsin, I would like to mention Dr.Salahuddin Zafar Bhai who has been very special to me. Dr Iqra Munir is also a wonderful lady and a great friend to me. After them, I would like to mention Faiqa Nazir Ahmad, Usama Adil, Usama Mirza, Muhammad Imran Nawaz, Amir Ali Joya, and all my cricketing and sports friends who provided me wonderful time here in bilkent.

# Contents

# List of Figures

# List of Tables

# Chapter 1

# Introduction

## 1.1 Introduction to two-dimensional materials

Since the discovery of graphene [2], two-dimensional (2D) materials have become the new confined quantum platforms to be explored for novel studies and applications. Numerous 2D materials can be found in all states of matter. For instance, graphene, molybdenum disulfide ($MoS_2$), and hexagonal boron nitride (hBN) are metal, semiconductor, and insulator respectively [2, 3, 4, 5]. These materials can either be grown using conventional methods like chemical vapor deposition (CVD) or can be exfoliated using standard mechanical exfoliation of a big crystal grown by chemical vapor transport (CVT) [5, 6, 7, 8, 9, 10, 11, 12]. All of the 2D materials are indeed confined quantum mechanical systems and need to be well studied to make their use in the real world at a large scale. There are several kinds of 2D materials, for example, some of them such as transition metal dichalcogenides (TMDCs), graphene, and hBN are layered. The layers of these materials interact with van der Waals forces [2, 13, 14]. Materials like $In_2S_3$ and $MoO_2$ can also be thinned down to a few layers (2D limit) but they are not layered because of a lack of van der Waals interaction between their layers, and hence these materials are not exfoliable [14, 15].

2D TMDCs are a wide range of materials that have exceptional optical, thermal, electrical, and mechanical properties. The general formula used to represent TMDCs is $MX_2$ where M indicates the transition metals such as titanium (Ti), vanadium (V), molybdenum (Mo), tungsten (W), tantalum (Ta), niobium (Nb), and platinum (Pt), etc and X represents chalcogenides such as sulfur (S), selenium (Se), and tellurium (Te) [5, 6, 16, 17, 18, 19, 20]. There are numerous 2D TMDC materials that can be found in various phases of the same material. For example, based on crystal structure, $MoS_2$ can be found in 2H, 3R, and 1T phases where 2H has a hexagonal structure, 3R has also a hexagonal structure with rhombohedral symmetry, and 1T has tetragonal symmetry [21, 22]. Different phases of the same material exhibit different properties. For example, the 2H and 3R phases of $MoS_2$ are semiconductors and the 1T phase shows a metallic nature although the metallic phase of $MoS_2$ is not very stable chemically in ambient conditions. Research is going on to make the 1T phase of $MoS_2$ more stable since it has its unique benefits and applications. Although many metallic phases of TMDC materials are not stable, still they have their applications. Some phases of TMDCs such as 2H phases of $MoS_2$, $MoSe_2$, $WS_2$, $WSe_2$, $TaS_2$, and $MoTe_2$ are chemically stable and have been extensively studied [23, 24, 25, 26].

## 1.2 Photoluminescence of TMDCs

An interesting phenomenon observed in $MoS_2$, $MoSe_2$, $WS_2$, and $WSe_2$ is the transition in the energy band gap from indirect to direct when thinned down to monolayers [27, 28, 29, 30, 31]. Hence, all these TMDCs are expected to show good photoluminescence (PL) spectroscopy signals. PL spectroscopy is an experimental technique used to see the optical response of materials. When a laser light of wavelength less than the emission wavelength of the material is shined onto a material, electrons are excited and go to the conduction band and a quasiparticle (known as neutral exciton) is formed with a hole in the valence band, and an electron in the conduction band as shown in figure 1.1. Upon recombination of hole and electron, a photon is emitted and captured by the detector which shows the response as a PL peak. This whole process is known as PL spectroscopy and

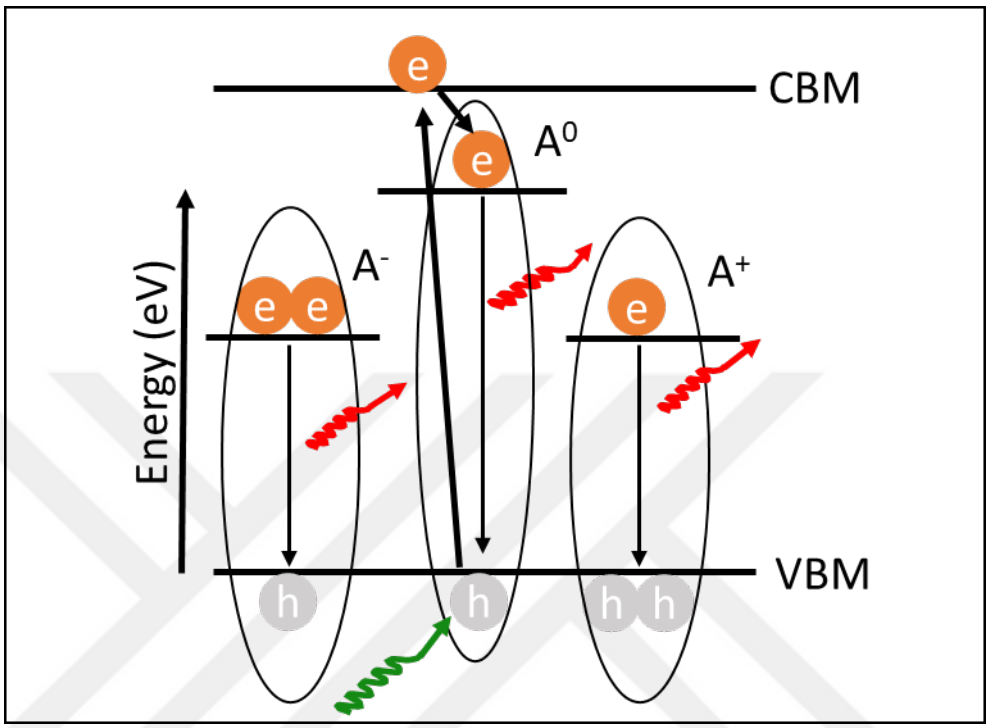


Figure 1.1: Schematic for PL emission from TMDCs. VBM and CBM denote valence band maximum and conduction band minimum egdes.

is very fruitful to see the optical transitions of materials experimentally in very little time. Apart from neutral excitons, some charged excitons (also known as trions) are also observed in experimental data and they can have both positive (formed by the Coulomb interaction of two holes and one electron) and negative charge (formed by the Coulomb interaction of two electrons and one hole) as shown in figure 1.1 depending on the formation (synthesis) and nature of the semiconductor. For instance, if a semiconducting TMDC is p-type in nature, there is a maximum probability that it will have some positive trions because of the presence of extra holes in that TMDC, and the same goes for an n-type semiconductor except the charge of trion which is negative in this case. The neutral excitonic recombination in the above mentioned TMDCs is symbolized as $A^0$ and trionic recombination is denominated by $A^{+/-}$. A trion has lower emission energy than an exciton because of a relatively weaker Coulomb interaction which is stronger in the case of neutral exciton [3, 32, 33, 34, 35, 36].

$MoS_2$ shows a tunable PL signal and is considered n-type in nature as reported

in many previous reports. Another interesting fact about $MoS_2$ is that it is the most defective among the above-mentioned 4 TMDCs providing a naturally tunable platform for optical as well as transport properties. It has some intrinsic sulfur vacancies and free electrons which reduce its PL peak intensity and make the peak broader with negative trion emission. Negative trions are even more intense in most of the reported crystals and we also observed the same in this study. Mechanically exfoliated monolayers of $MoS_2$ are considered less defective since they are cleaved layer by layer from a big crystal which has less probability of unwanted sulfur vacancies or other structural defects. However, they cannot be considered defect-free. Several ways to improve the quality of $MoS_2$ optical properties such as acid treatment, heterostructure formation with p-type dopant, or defect engineering have been reported. Here, we utilized the van der Waals gap and doping capability of metals to control the PL intensity, the trionic and excitonic recombinations, and the full-width at half maximum (FWHM) of $MoS_2$ [37, 38, 39, 40].

$WS_2$ shows a very robust emission of PL peak around 2.05 eV and has fewer defects compared to $MoS_2$. It is also reported as n-type in nature and has some free electrons which cause the formation of negative trions. Its PL intensity can also be enhanced or suppressed if placed with a suitable metal. As explained in figure 1.4 and later parts of the introduction, it is easier for high work function metals to inject holes into semiconducting TMDCs when there is a van der Waals gap. We also investigated the effect of the van der Waals gap, by performing the PL measurements before and after annealing the heterojunctions and successfully quenched the PL after annealing which clearly shows that the charge injection from metal to semiconductor depends on the van der Waals gap [30, 31].

For the case of $MoSe_2$, and $WSe_2$ we also investigated the effect of metal proximity on the PL emission of these two semiconducting TMDCs and obtained the results according to our expectations. We increased the number of positive trions in these materials by fabricating their heterostructures with high work function metals and reducing their overall PL emission [29, 30, 41, 42].

The reason behind this universal control of PL characteristics of TMDCs is

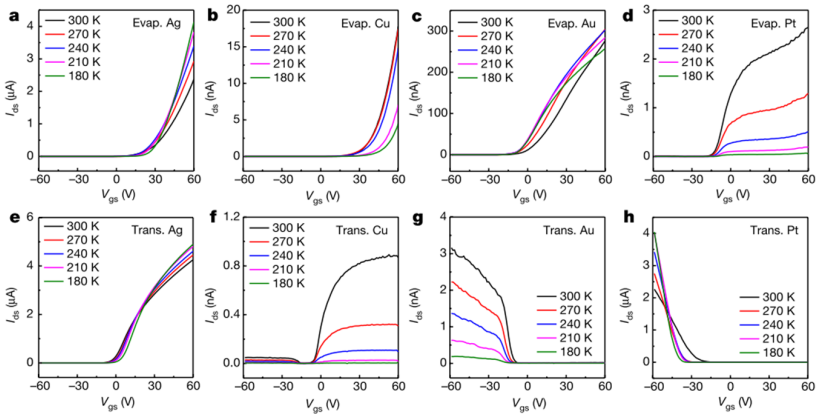


Figure 1.2: Transfer curves of 1L-$MoS_2$ based FETs and the top penal shows all the metals directly deposited on top of $MoS_2$ while lower panels show the transfer curves with transferred metallic electrodes (a) $MoS_2$ directly deposited with Ag contacts (b) $MoS_2$ directly deposited with Cu contacts(c) $MoS_2$ directly deposited with Au contacts(d) $MoS_2$ directly deposited with Pt contacts (e) Ag contacts transferred on top of $MoS_2$ (f) Cu contacts transferred on top of $MoS_2$ (e) Au contacts transferred on top of $MoS_2$ (e) Pt contacts transferred on top of $MoS_2$. Note: This figure is taken from [1] with permission

already explained in terms of device performance. For instance, as depicted in figure 1.2 when metals are directly evaporated on $MoS_2$ monolayer, it always exhibits an n-type behavior since the direct deposition of metal atoms can penetrate the surface of TMDC creating MIGS and FLP and providing the pathways for electrons to be easily transferred from metal to $MoS_2$ when a $V_{sd}$ is applied across the channel while applying vertical field simultaneously. However, when a high work function metal electrodes are fabricated and transferred on top of $MoS_2$ crystal, its contact polarity and nature of majority charge carriers are changed from n-type to p-type following the Schottky-Mott law which states that Schottky barrier height (SBH) for electrons increases with increasing metal work function and vice versa for holes as shown in figure 1.3. From here, we can infer that the transfer curve obtained in FETs does not only depend on the nature of the semiconductor (n-type, p-type, or ambipolar) but also depends on the type of contact between the semiconductor and metal electrode. Instead of direct deposition, if a metal electrode is transferred on top of a TMDC material, there remains some nanoscale gap around 0.3-0.5 nm known as the van der Waals gap [41, 43, 44].

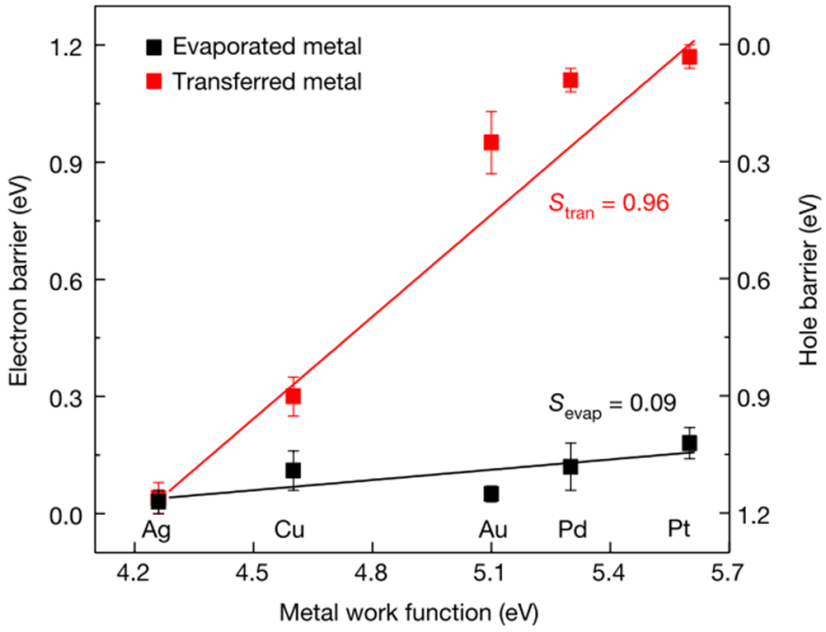


Figure 1.3: Metal work function vs Schottky barrier height (left for electron and right for holes). Note: This figure is taken from [1] with permission

SBH and van der Waals gap prohibit electrons from flowing to TMDCs from metals. Hence, whenever there is a van der Waals gap between TMDC and metal, the type of majority charge carriers depends on the work function of the metal [1, 19, 27, 37, 41, 45, 46, 47]. Most of the previous works focused mainly on device fabrication processes and enhancement of device performance. However, in this work, we carefully investigated the optical properties of various interfaces of TMDCs with several 2D/3D metals exploiting the van der Waals gap between the interfaces.

# Chapter 2

# Methods

## 2.1 Mechanical Exfoliation and Dry Transfer

In this technique, the process begins with a minute piece of a single source crystal delicately positioned onto a Scotch tape, named the master tape. The crystal is spread evenly across the surface of the tape. Subsequently, an additional piece of scotch tape is gently brought into contact with the master tape, repeating this process approximately 4-5 times. The primary objective is to reduce the thickness of the small crystal pieces over successive iterations as shown in figure 2.1 a. After the preparation of the tapes, a small piece of PDMS is placed on a glass slab and scotch tape is brought in contact with the PDMS stamp to transfer some crystals on PDMS as shown in figures 2.1 b and c respectively. This process is known as mechanical exfoliation.

Following the exfoliation of any TMDC material, PDMS is carefully observed under the optical microscope (OM) which is the quickest way to have an idea about the thickness of crystals as shown in figure 2.1 d. A suitable crystal is selected using OM. With the help of a glass slab holder shown in figure 2.1 d and a micromanipulator, the PDMS stamp is carefully brought in contact with the desired position of the substrate placed on the hot stage shown in figure 2.1 e.

A small piece of carbon tape is also placed beneath the substrate so that it may not move when PDMS is in contact with the substrate. This process is known as a dry transfer.

After the crystal is transferred to the substrate, the glass holder is replaced with a tungsten needle holder, and In source is also placed on the hot stage as shown in figure 2.1 f. A tiny needle is drawn from the molten In source which is at a higher temperature than the melting point of In metal (430 K) and is carefully placed on top of the desired position of the crystal as shown in figure 2.1 i. This is a very short and efficient way to fabricate 2-terminal devices. [1, 2, 11, 48, 49].

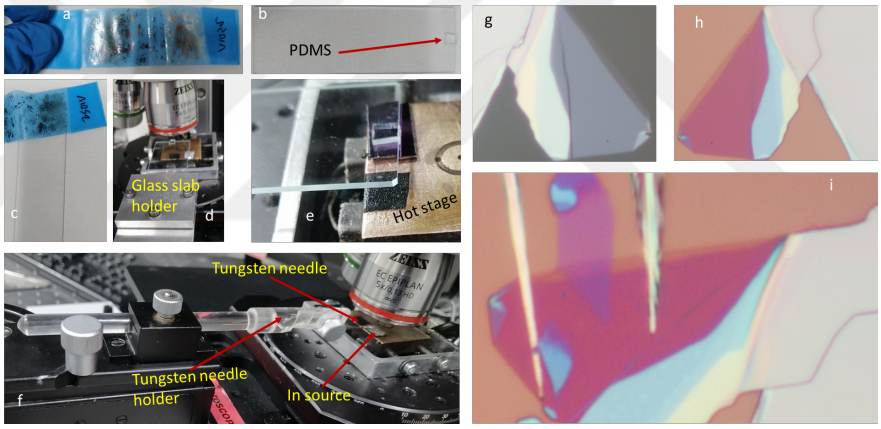


Figure 2.1: (a), (b), (c), (d), (e), and (f) are showing the images of scotch tape, PDMS placed on glass slab, scotch tape in contact with PDMS stamp, PDMS under optical observation, PDMS in contact with desired substrate, and In needle contacts placement on crystals taken by mobile phone camera. (g) OM image of a suitable crystal found on PDMS by OM observation. (h) OM image of the same crystal transferred on $SiO_2$/Si substrate and (i) shows the OM image of 2-electrode device formed on the same crystal.

## 2.2 Substrate preparation

We used various substrates in this work which are explained in this section. We used 300 nm $SiO_2$ coated Si chips. Since the $SiO_2$ layer is insulating in nature and can be utilized as a conventional gating material to apply an external electric field which is used to modulate various properties of 2D materials. To avoid leakage

of charges (pinhole effect), we deposited a 30 nm layer of alumina ($Al_2O_3$) using atomic layer deposition (ALD). We also used sapphire substrates which are also insulating in nature providing a platform to perform electrical measurements of the materials. To see the metal-semiconductor interaction, we also prepared some conducting substrates, by using a thermal evaporator. We deposited 10/100 nm of Cr/Au, and 30 nm of Ag on insulating substrates such as $SiO_2$/Si or sapphire chips to have a metallic background under semiconductors. We also used a precision etching coating system to coat a 30 nm thick layer of Pt on $SiO_2$/Si substrate. All the chips were carefully cleaned using Acetone, Isopropanol, and DI water and then dried using a nitrogen gun. [50, 51, 52].

## 2.3 Photoluminescence and Raman spectroscopy

PL spectroscopy is a universal, powerful, non-contact, non-destructive, efficient, user-friendly, and time-saving characterization technique to explore the optical properties of semiconductors. It provides detailed information about the light emission properties and band gap of the semiconducting materials. In this technique, a focused laser light with higher energy than the semiconductor's band gap is directed onto the sample, exciting electrons from the valence band to the semiconductor's conduction band. As these charges relax, they emit a light signal, which is then detected by a sensor, revealing a PL peak. This peak offers insights into the recombination of charge carriers, elucidating the mechanism and nature of light emission.

For example, $MoS_2$ emits light at a wavelength of around 660 nm through a direct transition, a distinctive feature indicative of its monolayer structure. PL spectroscopy also proves useful for thickness analysis of many 2D materials, since a bilayer does not exhibit the same emission wavelength as a single layer. [32, 33, 34].

The experimental setup shown in figure 2.2 can be used for PL and Raman spectroscopy. Raman spectroscopy is a powerful characterization technique used

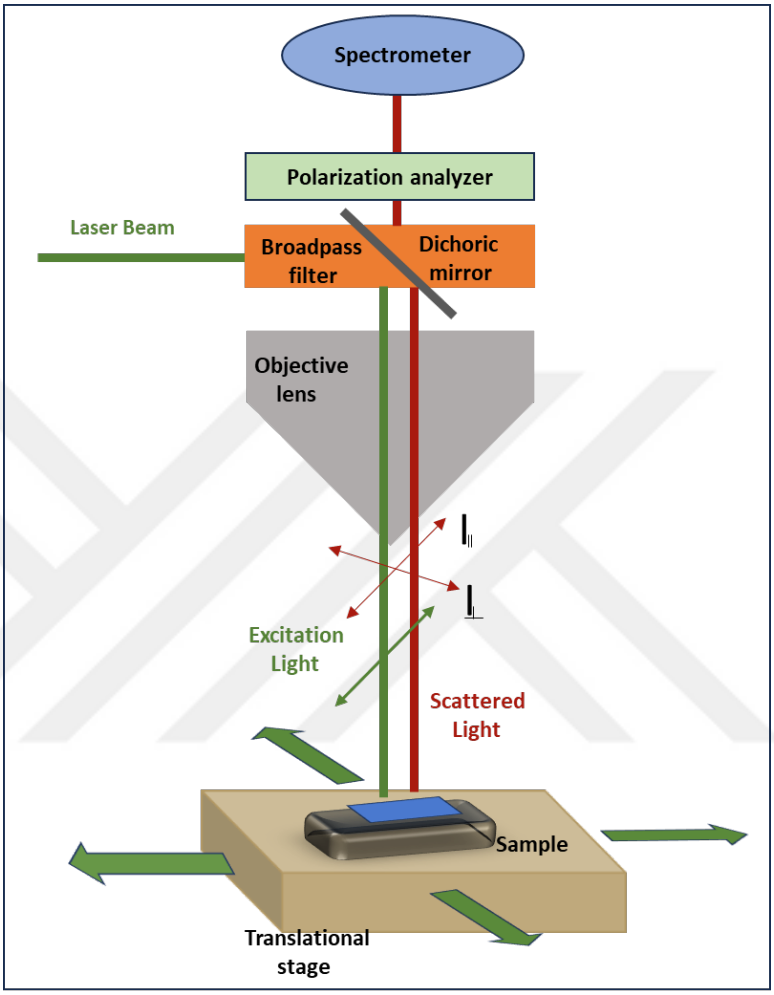


Figure 2.2: Schematic for PL and Raman Spectroscopy set up

to analyze the chemical composition of materials by determining the vibrational modes of molecules. A source of monochromatic light typically a 532 nm laser source is used for light production. A fully focused laser beam by objective lens interacts with the sample's molecular vibrations, phonons, or other excitations. Light gets scattered when it interacts with the sample. The scattered light has a higher wavelength than the incident laser because of the interaction with the sample. The elastically scattered light is filtered out and the remaining light is sent to the Raman spectrometer which collects the signal and provides the fingerprints of molecules showing various peaks of distinct frequencies corresponding to specific materials. For instance, $MoS_2$ has several Raman active modes, but the most dominant are $A_{1g}$ and $E^1{}_{2g}$ which are detected at the frequencies of 385 $cm^{-1}$

and 405 $cm^{-1}$ respectively for a monolayer. Raman spectroscopy can also be used for thickness measurements of 2D materials because its signal is also sensitive to thickness. It is a very easy, time-saving, efficient, and robust material identification technique that does not require even a very complex setup and analysis of the data [53, 54].

# Chapter 3

# Vertical heterostructures of molybdenum-based chalcogenides with 2D/3D metals

## 3.1 Introduction

$MoS_2$ and $MoSe_2$ are 2D TMDCs owing a transition of band gap from indirect to direct when thinned down to a monolayer [28, 29]. There are several ways to see this transition i.e. PL spectroscopy and Raman Spectroscopy [55]. If PL emission is near 660 nm and 820 nm for $MoS_2$ and $MoSe_2$ respectively, it is direct evidence of band gap transition. PL peak position, shape, and intensity are the parameters to guess the thickness of crystals. For instance, the peak position of $MoS_2$ is between 655 and 660 nm for a monolayer and if the peak is centered around 670 nm, this is clear evidence that the crystal is a bilayer. Raman spectroscopy is also good in terms of thickness analysis of TMDC crystals. For example, if the difference between peak positions of $A_{1g}$ and $E^1{}_{2g}$ Raman modes of $MoS_2$ is less than 20 $cm^{-1}$, this is a signature that the crystal is a monolayer. Moreover, this difference between frequencies of in-plane and out-of-plane modes increases with increasing thickness [56, 57]. We did both the Raman

and PL characterizations to show the presence of monolayers of these TMDCs and then fabricated heterostructures with strategically chosen metals such as $TaS_2$, $NbTe_2$, graphene, and Au to control (enhance or suppress) the intensity of PL. We investigated the substrate effect as well as different configurations of these hetero-structures. In addition to room temperature PL measurements at these interfaces, we also did temperature, perpendicular electric field, and excitation power-dependent PL measurements to explain the mechanism.

## 3.2 Photoluminescence enhancement

In this section, we will explain PL enhancement at various vertical van der Waals heterostructures including $TaS_2/MoS_2$ and $MoS_2/NbTe_2$ on various insulating and conducting substrates to show the substrate effect, and these interfaces were fabricated at arbitrary angles to eliminate any geometrical dependence on PL enhancement. Moreover, we performed back gate-dependent and temperature-dependent PL measurements to show the control on the enhanced PL intensity, and to explain the underlying recombination mechanism, we reported pump power-dependent measurements of PL at interfaces and bare $MoS_2$.

### 3.2.1 $MoS_2$ and $TaS_2$ heterostructures

#### 3.2.1.1 $MoS_2$ and $TaS_2$ heterostructures on insulating substrates

Heterostructures consisting of $MoS_2$ and $TaS_2$ were carefully fabricated on 30nm alumina ($Al_2O_3$) coated $SiO_2$/Si substrates, using mechanical exfoliation and dry transfer techniques demonstrated in detail in methods. The reason behind the passivization layer of 30 nm $Al_2O_3$ is to avoid the pinhole effect. To compare PL characteristics of bare $MoS_2$, and hetero-structure, we partially placed $MoS_2$ monolayer on top of $TaS_2$ or $TaS_2$ on top of $MoS_2$ monolayer.

In Figure 3.1, two configurations of $MoS_2$ and $TaS_2$ hetero-structures are presented for comparative analysis. In figure 3.1 an optical microscope (OM) image of heterostructure showing 1L-$MoS_2$ placed above a few layers thick $TaS_2$ crystal. Figure 3.1 b corresponds to figure 3.1 a showing the PL spectroscopy map of the heterostructure, demonstrating consistent PL enhancement throughout the junction area, and figure 3.1 c provides a PL point spectrum data from both bare $MoS_2$ and hetero-structure part. Upon deconvolution of the data using Lorentzian fitting through Origin Software and equation 3.1, the obtained data reveals that the contribution to PL emission intensity from $A^-$ (trions) is reduced significantly at the interface compared to bare $MoS_2$ in contrast to $A^0$ (excitons) which are strongly enhanced at the interface as compared to bare $MoS_2$. Trions are indeed, inherent in $MoS_2$ due to defects such as sulfur vacancies and free electrons [35, 36, 58, 59].

$$y = y_0 + \frac{2A}{\pi}\left(\frac{\omega}{4(x - x_c^2)} + \omega^2\right) \tag{3.1}$$

Where $x$, and $y$ are variables and $y_0$, $A$, $\omega$, and $x_c$ denote initial position along y, the area under the curve, and full width at half maximum (FWHM). We preferred the Lorentzian fitting over the Gaussian because it provides more pronounced tails, and there is a lower probability of misleading from the fitting as compared to the Gaussian fitting [60].

| | | $MoS_2$ (top) | $MoS_2/TaS_2$ | $MoS_2$ (bottom) | $TaS_2/MoS_2$ |
|---|---|---|---|---|---|
| Peak Position (eV) | $A^-$ | 1.8504 | 1.87021 | 1.85669 | 1.86762 |
| | $A^0$ | 1.88936 | 1.89574 | 1.89101 | 1.89461 |
| | B | 2.00868 | 2.03749 | 2.01837 | 2.0334 |
| Area/$A_{tot}$ | $A^-$ | 0.4651 | 0.2482 | 0.419 | 0.387 |
| | $A^0$ | 0.4474 | 0.7488 | 0.533 | 0.597 |
| | B | 0.087 | 0.00295 | 0.048 | 0.015 |
| FWHM (meV) | $A^-$ | 83 | 71 | 82 | 68 |
| | $A^0$ | 65 | 45 | 60 | 46 |
| | B | 87 | 18 | 69 | 36 |

Table 3.1: This table corresponds to figure 3.1 showing the quantitative analysis of all quasi particles ($A^-$, $A^0$, B) in bare $MoS_2$, and hetero-structures.

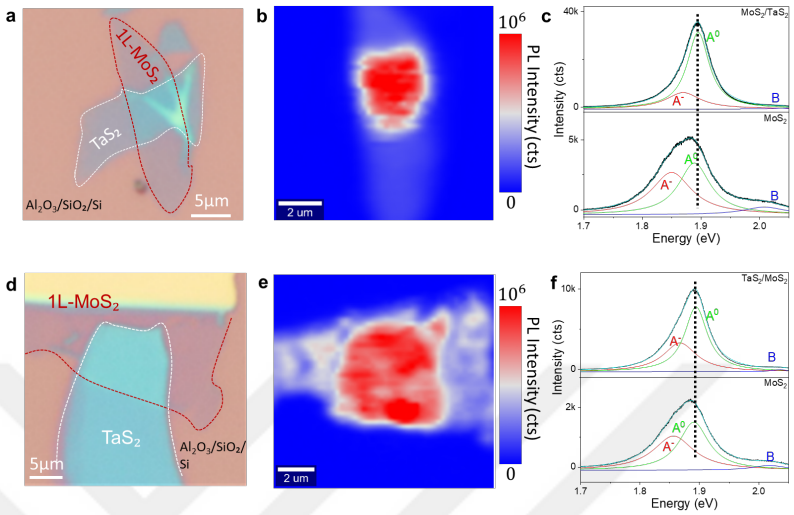


Figure 3.1: (a) OM image of hetero-structure with $MoS_2$ on top of $TaS_2$ on 30nm alumina coated $SiO_2$/Si substrate (b) PL map corresponding to hetero-structure in a (c) PL point spectrum of $MoS_2$ and hetero-structure (d) OM image of hetero-structure with $TaS_2$ on top of $MoS_2$ on 30nm alumina coated $SiO_2$/Si substrate (e) PL map corresponding to hetero-structure shown in d (f) PL point spectrum of $MoS_2$ and hetero-structure

The suppression of trion intensity is attributed to p-type doping from $TaS_2$, irrespective of whether $MoS_2$ is positioned above or below. Despite $TaS_2$ being a metallic 2D material, its high work function ($\approx 5.6eV$) [61] induces hole generation, due to a van der Waals gap between $MoS_2$ and $TaS_2$ surfaces [1, 19, 27, 43, 46, 55, 62]. This not only reduces trion numbers but also amplifies overall excitons $A^0$, as quantitative data of both configurations is shown in Table 3.1. The B exciton, which also arises from the direct transition of electrons but has a little bit higher energy than $A^0$ [35, 63, 64] and has less probability to occur because most of the transition takes place as $A^0$ and it further diminishes at the $MoS_2$-$TaS_2$ interface in insulating substrates.

Moreover, peak positions at the interfaces shift towards higher energies due to an increased population of excitons, while FWHM values for all peaks decrease, indicating improved PL emission and reduced contributions from defects [46, 38, 39]. In Figures (d), (e), and (f), optical microscopy images of $TaS_2$ on top of $MoS_2$, its corresponding PL map, and PL point spectra are demonstrated respectively, exhibiting similar behavior as expressed by the first configuration.

We also fabricated a heterostructure of $TaS_2$ on top of $MoS_2$ on sapphire which is another insulating substrate used commonly in the community and results are presented in figure 3.2 and table 3.2. There is no qualitative difference in our observations of PL enhancement on $SiO_2$/Si and sapphire. It can be inferred from this section, that there is not any influence of the geometry of heterostructure since all three different samples formed at random angles show similar results. This is also clear from this section that insulating substrates yield similar results. [1, 19, 40, 42, 43, 46, 55, 65, 66, 67, 68].

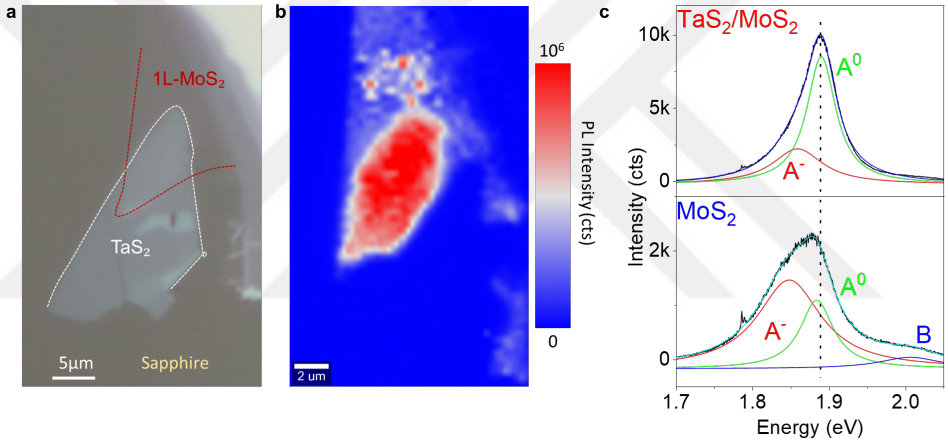


Figure 3.2: (a) OM image of hetero-structure with $TaS_2$ on top of $MoS_2$ on sapphire (b) PL Map (c) PL point spectrum of $MoS_2$ and hetero-structure

| | | $MoS_2$ | $MoS_2/TaS_2$ |
|---|---|---|---|
| Peak Position (eV) | $A^-$ | 1.84825 | 1.85544 |
| | $A^0$ | 1.8843 | 1.88699 |
| | B | 2.00868 | 2.02358 |
| Area/$A_{tot}$ | $A^-$ | 0.66 | 0.326 |
| | $A^0$ | 0.26 | 0.666 |
| | B | 0.08 | 0.008 |
| FWHM (meV) | $A^-$ | 102 | 82 |
| | $A^0$ | 52 | 46 |
| | B | 95 | 31 |

Table 3.2: This table corresponds to figure 3.2 and displays the quantitative analysis of all quasi-particles ($A^-$, $A^0$, and B)

#### 3.2.1.2 Excitation power dependent PL measurements

Excitation power-dependent PL measurements were conducted on the heterostructure illustrated in Figure 3.1 a. Upon deconvoluting the acquired data using equation 3.1 and plotting laser power versus peak intensity on a log-log scale, the fitting parameters, denoted as $\alpha_{MoS_2}$ and $\alpha_{hetero}$ provide insights into the recombination mechanisms occurring in both bare $MoS_2$ and the hetero-structure.

In the case of bare $MoS_2$, where $0 < \alpha_{MoS_2} < 1$, the fitting parameter suggests non radiative recombinations. Conversely, $1 < \alpha_{hetero} < 2$ in the heterostructure indicates that excitonic recombinations predominantly occur at the interface of $MoS_2$ and $TaS_2$ [69, 70, 71, 72, 73, 74]. Another interesting observation in these measurements is the PL enhancement in both bare $MoS_2$ and the heterostructure with increasing power. This enhancement in PL with laser power can be attributed to the increased number of incident photons interacting with the semiconductors [75, 74]. The elevated excitation leads to an increased population of excited charge carriers, resulting in more recombination events upon relaxation. Consequently, enhancing the PL intensity and revealing the distinct recombination mechanisms in both the interface and bare $MoS_2$. The fitting was done using equation 3.2 (power law) through Origin Software.

$$y = ax^{\alpha} \tag{3.2}$$

Where, $a$, $x$, $y$, and $\alpha$ denote proportionality constant, laser power, PL intensity, and fitting parameter respectively. This analysis not only explains the underlying mechanisms of recombination in the heterostructure and bare $MoS_2$ but also demonstrates the impact of excitation power on the optical properties of both bare $MoS_2$ and the $MoS_2/TaS_2$ interface.

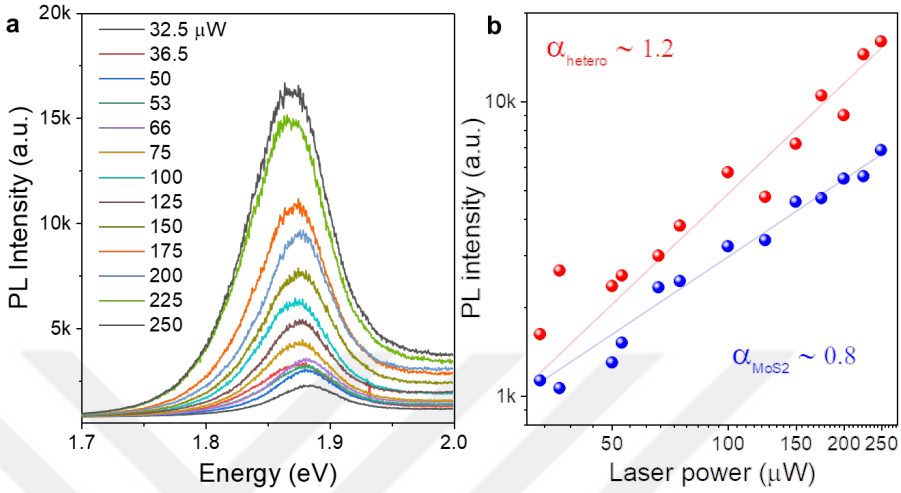


Figure 3.3: (a) Pump power dependent PL measurement of hetero-structure (b) Integrated PL intensity vs laser power on a log-log scale

#### 3.2.1.3 Gate-dependent PL measurements

One way to control the PL intensity and charge carrier concentration is by applying the back gate voltage [1, 3, 16, 35, 76, 77]. Figure 3.3 a shows the schematic of a device fabricated to perform PL measurements under an external electric field applied perpendicular to the plane of the heterostructure. The heterostructure was fabricated on a positively doped Si substrate coated with a 300 nm $SiO_2$ layer. $SiO_2$ layer was scratched carefully to apply the gate voltage and an Indium needle was placed on top of $MoS_2$ for grounding. The method to place indium contact is very well explained in our previous reports [48, 49].

When the negative gate voltage is applied, electrons are depleted from $MoS_2$ and hence there is low electron density in $MoS_2$ leading to suppression in the number of trions and free electrons which ultimately enhances the excitonic population resulting in a blue shift to the peak position and enhancement in the intensity of PL emission from both $MoS_2$ and heterostructure as depicted in figure 3.3 b (contour plot) as well as figure 3.3 f [3, 35]. When a positive gate voltage is applied, electrons are injected into $MoS_2$, and with increasing positive gate voltage, the concentration of electrons increases resulting in an increase in the number of trions and reducing the number of excitons which leads to a red

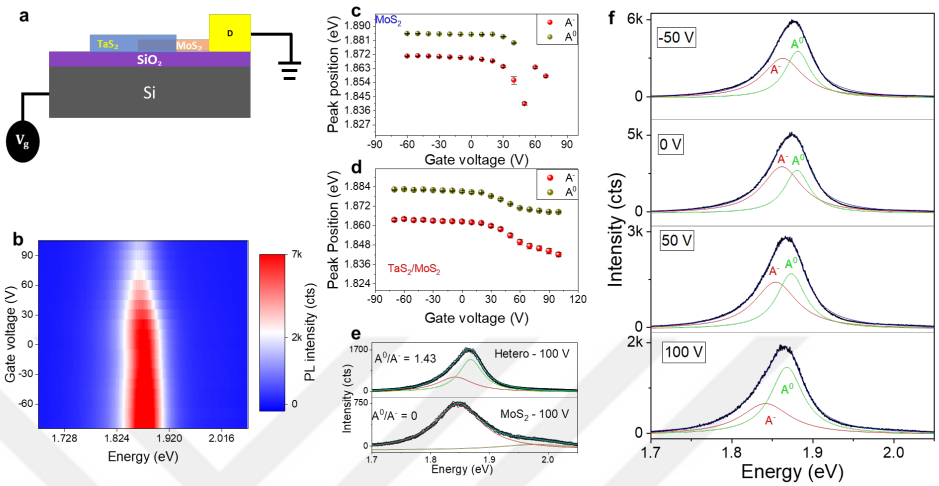


Figure 3.4: (a) Schematic for back gated device(b) PL contour map showing the change in peak position of PL intensity by changing gate voltage and scale bar on the right side of contour map shows PL intensity (c) Peak position of $A^0$ and $A^-$ in $MoS_2$ with the change in gate voltage (d) Peak position of $A^0$ and $A^-$ in heterostructure with the change in gate voltage (e) PL point spectrum at 100 V from both bare $MoS_2$ and hetero-structure indicating the persistent $A^0$ exciton in heterostructure which is absent in bare $MoS_2$ (f) PL at various gate voltages from heterostructure

shift in the peak position of $MoS_2$ and PL suppression due to fewer excitonic recombination. This has been already reported in many reports for the case of $MoS_2$ and even other semiconducting TMDCs such as $WS_2$, and $WSe_2$. Trions are the particles that are robust in $MoS_2$ and do not vanish even the higher negative gate voltages are applied because they are formed due to defects such as sulfur vacancies, free electrons, and some structural defects.

This gets very interesting if we park the laser on the heterostructure part and apply positive gate voltage. $TaS_2$ acts as a source for hole injection to $MoS_2$ in contrast to back gate voltage which acts as a source for electron injection to $MoS_2$. As electrons are being injected into $MoS_2$, their impact is being nullified to some extent by holes provided by $TaS_2$ and hence we obtain some excitons even when we are applying 100 V of back gate voltage though the intensity of PL peak is suppressed as compared to negative gate voltage as indicated in figure 3.4 d, and e. These persistent excitons have not been observed and realized before.

The proximity of $TaS_2$ and hole injection from $TaS_2$ is the reason behind this persistent excitonic recombination. This new exciting observation provides the pavement for novel optoelectronic devices which has not been observed before [1, 3, 16, 35, 76, 77].

#### 3.2.1.4 Temperature dependent PL measurements on insulating substrates

Temperature is one of the most influential parameters whenever we talk about any condensed matter physics phenomenon. If we decrease the temperature and perform PL measurements, many new peaks appear for the $MoS_2$ case and they are attributed to defect peaks, or biexcitons (a quasi-particle composed of 2 holes and 2 electrons) [40, 59, 78, 79]. We performed temperature-dependent PL measurements on the same heterostructure shown in figure 3.1 a. It was observed that from 3.5 K to room temperature (293K), the PL intensity of $MoS_2$ was decreasing with temperature as it is clear from figure 3.5 c that the integrated PL intensity is decreasing throughout all temperatures.

However, the trend was different for heterostructures as it is obvious in figure 3.5 c. After merging with bare $MoS_2$ PL intensity, it started increasing after 250 K and kept on increasing with temperature until room temperature. This changing trend in PL intensity was also observed from another heterostructure of the same configuration. These observations from two distinct samples provide the reproducibility and reliability of our results.

The enhancement in PL of heterostructures can be attributed to the reduction in spectral weight of biexcitons ($A_{xx}$) beyond 250 K. This phenomenon suggests that the thermal energy, facilitated by an increase in temperature, might play an important role in breaking down $A_{xx}$ into trions and excitons. Notably, the observed trend indicates a threshold temperature of 250 K, beyond which there is a noticeable decline in the overall areal percentage of $A_{xx}$, as illustrated in Figure 3.5 a, c, and d. This shift in spectral weight and areal percentage highlights the influence of temperature as a key factor in modulating the optical properties of

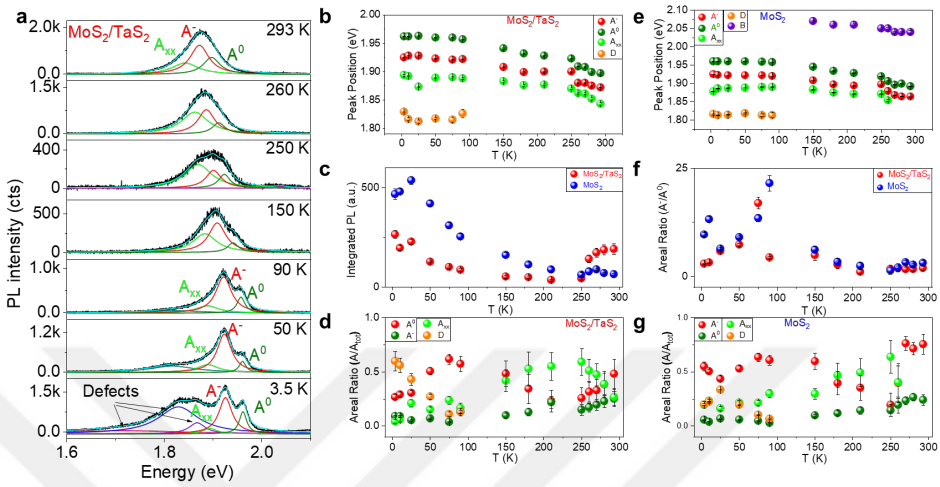


Figure 3.5: (a) PL point spectrum of heterostructure at various temperatures from 3.5 K to room temperature showing PL quenching as the temperature increases until 250 K, and after 250 K, PL starts increasing (b) Peak positions of all quasi-particles present in heterostructure, D is observed at low temperatures but $A_{xx}$ is to room temperature in heterostructure (c) Integrated PL intensity of heterostructure and bare $MoS_2$ showing an anomalous behavior in the interface after 250 K (d) Areal ratio is a ratio between the area of the quasi-particles and total area of PL peaks and $A_{xx}$ is reducing after 250 K with increasing weights of trions and excitons (e) Peak positions of all quasi-particles in bare $MoS_2$ (f) Areal ration of trion and exciton showing $MoS_2$ has always higher no of trionic recombinations than in hetero-structure (g) Areal ratio of all quasi-particles in bare $MoS_2$

the heterostructure, particularly in the context of $A_{xx}$ dynamics [40, 59, 78, 79].

#### 3.2.1.5 $MoS_2$ and $TaS_2$ heterostructures on gold substrate

Gold (Au) is a high work function metal (≈5.1 eV) and if 1L-$MoS_2$ is transferred on top of Au, it can dope $MoS_2$ with holes and can cause the enhancement in PL intensity of $MoS_2$ when compared with PL intensity of $MoS_2$ placed on PDMS. As already explained in section 3.2.1, the van der Waals gap causes holes to tunnel through $MoS_2$-1L, and the exciton's intensity is increased in contrast to the reduction in trions emission intensity. After obtaining the PL from $MoS_2$, we transferred a few layered $TaS_2$ partially on top of $MoS_2$, and due to more charge

transfer, we realized further uniform enhancement in PL intensity of $MoS_2$ part sandwiched between Au and $TaS_2$ as compared to the part placed only on Au as shown in figure 3.6 b and f [78, 80].

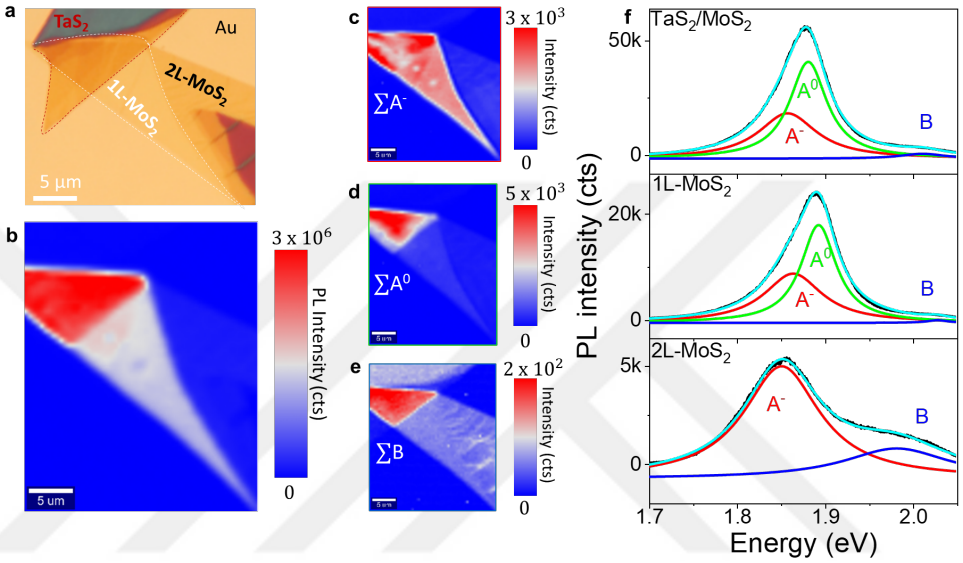


Figure 3.6: (a) OM image of hetero-structure with $TaS_2$ on top of $MoS_2$ on 100 nm gold coated $SiO_2$/Si substrate(b) PL Map (c) PL map focused on peak position of trion $A^-$ (d) PL map focused on peak position of exciton $A^0$ (e) PL map focused on peak position of exciton B (f) PL point spectrum plot showing 2L-$MoS_2$, 1L-$MoS_2$, and hetero-structure

We did further analysis of each quasi-particle by focusing on PL-mapped data near the peak positions of all three quasi-particles $A^0$, $A_-$, and B. It can be seen from figure 3.6 c that trions are spread all over the $MoS_2$ single layer with more trions in the sandwiched part of $MoS_2$. Figure 3.6 d shows that excitons are more localized and intense in the sandwiched part of $MoS_2$. It is quite strange that B excitons are also enhancing when we compare with $MoS_2$ on PDMS or the heterostructures formed at the insulating substrates which need to be explored more. Moreover, B exciton is localized in the sandwiched part of $MoS_2$. We have also shown the PL of bilayer $MoS_2$ which is very low in magnitude as compared to monolayer and secondly, it has only trions and no $A^0$ exciton with a few B excitons in agreement with previous reports. Reflection of light can also cause enhancement in PL but it can not add any specific recombination such as

excitons or trions. It enhances the overall PL which adds to small changes in PL enhancement. Mainly, it's the hole injection from both Au and $TaS_2$ that causes this huge enhancement in PL intensity and provides a new platform for optoelectronic devices [1, 19, 40, 42, 43, 46, 55, 68, 78, 80, 81].

| | | $MoS_2$ (monolayer) | $MoS_2/TaS_2$ | $MoS_2$ (bilayer) |
|---|---|---|---|---|
| Peak Position (eV) | $A^-$ | 1.84255 | 1.84605 | 1.83865 |
| | $A^0$ | 1.87509 | 1.87613 | N/A |
| | B | 2.0009 | 2.0013 | 1.93755 |
| $Area/A_{tot}$ | $A^-$ | 0.4461 | 0.4068 | 0.725 |
| | $A^0$ | 0.5453 | 0.5591 | N/A |
| | B | 0.0087 | 0.034 | 0.275 |
| FWHM (meV) | $A^-$ | 80 | 78 | 102 |
| | $A^0$ | 46 | 45 | N/A |
| | B | 30 | 60 | 140 |

Table 3.3: This table corresponds to figure 3.6 showing quantitative analysis of all quasi-particles obtained from Lorentzian fitting of PL data shown in figure 3.6 f.

#### 3.2.1.6 Temperature dependent PL measurements of $MoS_2$ and $TaS_2$ heterostructures on gold substrate

We did temperature-dependent PL measurements of heterostructure shown in figure 3.7 a. In contrast to our previous observations of low-temperature PL measurements on an insulating substrate, as discussed in section 3.5, we obtained enhanced PL from the sandwiched part of $MoS_2$ as compared to the Au part across all temperature ranges from 3.5 K to 293 K. We also observed less number of defective peaks at lower temperatures due to substrate effect. In contrast to our previous observations, we did not observe any biexciton or defect-related peaks at room temperature in these measurements. It is obvious that when we encapsulate $MoS_2$ in between two metals while maintaining the van der Waals gap which is compulsory for hole injection, PL is enhanced at all temperatures as it is depicted in figure 3.8. The possible reasons for this throughout enhancement of PL at the interface can be the hole injection from both $TaS_2$, and Au with light scattering from the gold surface because Au surface reflects the light and

can cause the enhancement in PL as it is already explained in ref 88, and 90 [1, 19, 40, 42, 43, 46, 55, 68, 78, 80, 81].

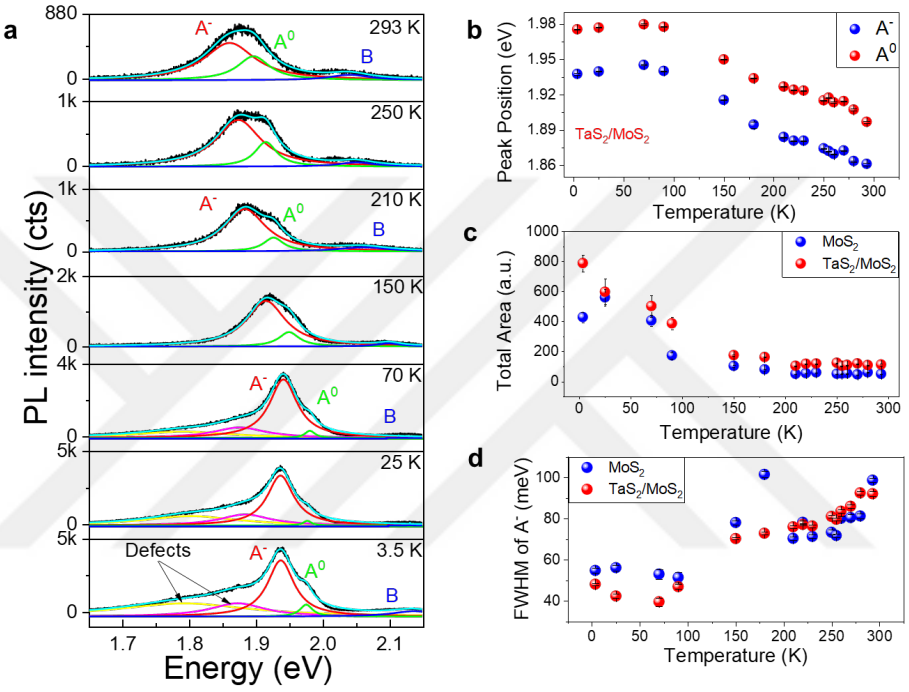


Figure 3.7: (a) PL point spectrum of heterostructure at various temperatures from 3.5 K to room temperature (b) Peak positions of $A^-$, and $A^0$ in heterostructure (c) Integrated PL intensity of heterostructure and bare $MoS_2$ showing more PL emission from the interfaced part at all temperatures (d) FWHM of $A^-$ in $MoS_2$ and heterostructure showing the overall enlargement with temperature as expected

### 3.2.2 $MoS_2$ and $NbTe_2$ heterostructure

Following our experiments with $TaS_2$, we proceeded to interface $MoS_2$ with $NbTe_2$, another metallic 2D material, with a work function of (5.32 eV) to validate the consistency of our findings. The results reinforced our initial understanding of van der Waals interfaces, as we observed a similar enhancement in PL at this interface as well. This is clearly illustrated in figure 3.8 c and table 3.4 that the interface has more intense PL emission as compared to bare $MoS_2$ although the

enhancement is not as robust as observed for the case of $TaS_2$. There can be several reasons such as the stability of $NbTe_2$, thickness of $NbTe_2$ crystal, and sapphire peaks which are dominating the bare $MoS_2$ PL measurements affecting the Lorentzian fitting for less enhancement factor at the $MoS_2/NbTe_2$ interface. Due to sapphire peaks, we probably obtained more enhancement in trions as compared to excitons at the interface although both contributed to PL enhancement in the end. B exciton is also suppressed at the interface as expected on insulating substrates [1, 82, 83].

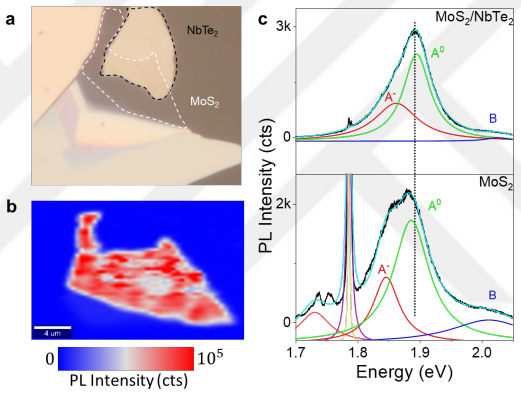


Figure 3.8: (a) OM image of $MoS_2$ partially placed on $NbTe_2$, and sapphire substrate (b) PL map (c) PL point spectrum showing PL enhancement at the interface of $MoS_2$ and $NbTe_2$

| | | $MoS_2$ | $MoS_2/NbTe_2$ |
|---|---|---|---|
| Peak Position (eV) | $A^-$ | 1.84621 | 1.86326 |
| | $A^0$ | 1.88677 | 1.89552 |
| | B | 2.01182 | 2.02604 |
| $Area/A_{tot}$ | $A^-$ | 0.218 | 0.35 |
| | $A^0$ | 0.561 | 0.629 |
| | B | 0.221 | 0.021 |
| FWHM (meV) | $A^-$ | 51 | 82 |
| | $A^0$ | 70 | 53 |
| | B | 148 | 44 |

Table 3.4: This table corresponds to figure 3.8.

## 3.3 Photoluminescence suppression

So far in this chapter, we explained several results showing PL enhancement at the vertical van der Waals interfaces. From here on, PL suppression will be demonstrated at various interfaces such as $MoS_2$/graphene, $TaS_2$/$MoSe_2$, and $MoSe_2$/Au to support our claim of universal control of PL characteristics.

### 3.3.1 $MoS_2$ and graphene heterostructure

Graphene is a 2D metallic material and has very interesting properties in its intrinsic form. Because of its low work function (4.30 eV), it can be used as an electron donor to $MoS_2$ which we experimented on and the results were according to our expectations. PL intensity was greatly reduced in the interfaced part of $MoS_2$ under graphene as compared to bare $MoS_2$ as shown in figure 3.9 and table 3.5. It is demonstrated in table 3.5 and figure 3.9 b that $A^0$ exciton vanishes at the interface and we are left with only trionic recombinations happening at the interface suggesting strong n-type doping to $MoS_2$ from graphene doping[1, 2, 3, 19, 80, 84, 85].

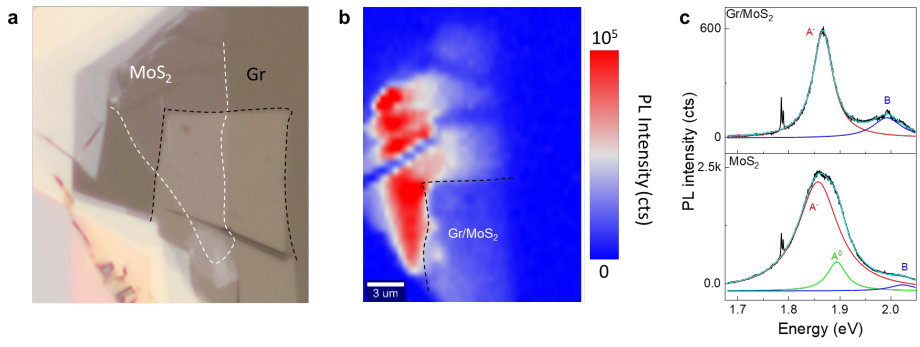


Figure 3.9: (a) OM image of graphene placed on top of some part of $MoS_2$ (b) PL map (c) PL point spectrum showing PL suppression at the interface of $MoS_2$ and graphene and indicating the enhancement of trion and complete suppression of excitons

| | | $MoS_2$ | $Gr/MoS_2$ |
|---|---|---|---|
| Peak Position (eV) | $A^-$ | 1.85797 | 1.85911 |
| | $A^0$ | 1.89352 | N/A |
| | B | 2.02071 | 1.99603 |
| $Area/A_{tot}$ | $A^-$ | 0.732 | 0.96 |
| | $A^0$ | 0.214 | N/A |
| | B | 0.054 | 0.04 |
| FWHM (meV) | $A^-$ | 97 | 80 |
| | $A^0$ | 55 | N/A |
| | B | 73 | 32 |

Table 3.5: This table corresponds to figure 3.9.

### 3.3.2 $TaS_2$ and $MoSe_2$ heterostructure

$MoSe_2$ is a semiconducting TMDC material and possesses a direct gap when thinned down to a monolayer. It has a lower bandgap (1.6 eV) than its sulfide counterpart. It has some selenium vacancies as sulfur vacancies in $MoS_2$. However, these vacancies are filled by air or oxygen molecules and the density of defects or vacancies is less than $MoS_2$. This material has also been very well studied because of its unique properties.

Here, we focused mainly on the PL of bare $MoSe_2$ and its heterostructure with TaS2. When $MoSe_2$ is interfaced with $TaS_2$, a metal that has a higher work function than, it results in p-type doping to $MoSe_2$. This increases the number of positive charge carriers, leading to significant suppression of PL compared to bare $MoSe_2$ or $MoSe_2$ on PDMS. The majority of charge carrier transportation of $MoSe_2$ depends on the metal work function used as electrodes and device fabrication method. Whenever a high work function metal is transferred on top of $MoSe_2$, the holes are transferred from metal to $MoSe_2$, and its doping level changes causing abrupt changes in its optical properties. Here, we observed the suppression in PL intensity of $MoSe_2$ when it was interfaced with $TaS_2$ because positive trions were formed at the interface due to holes injection from $TaS_2$. The quenching in PL of the $TaS_2/MoSe_2$ interface is shown in figure 3.10 and the quantitative analysis of individual quasi-particles is demonstrated in table 3.6 [17, 29, 86, 87].

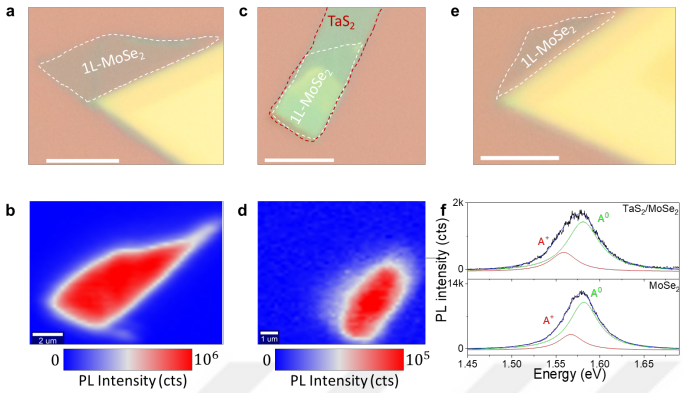


Figure 3.10: (a) OM image of $MoSe_2$ placed on top of 30 nm alumina coated $SiO_2$/Si substrate (b) PL map from the monolayer of $MoSe_2$ only (c) OM image of $TaS_2$ on top of $MoSe_2$ on 30 nm alumina coated $SiO_2$/Si substrate (d) PL map of interface showing uniform signal but intensity was lower than bare $MoSe_2$ (e) OM image of remaining part of $MoSe_2$ (f) PL point spectrum at the bare $MoSe_2$ and interface showing the suppression in PL peak intensity and enhancement in positive trion intensity. Scale bar in a,c, and e is 5 µm

| | | $MoSe_2$ | $TaS_2/MoSe_2$ |
|---|---|---|---|
| Peak Position(eV) | $A^+$ | 1.565979 | 1.5593 |
| | $A^0$ | 1.58121 | 1.5822 |
| $Area/A_{tot}$ | $A^+$ | 0.21 | 0.24 |
| | $A^0$ | 0.79 | 0.76 |
| FWHM (meV) | $A^+$ | 37 | 33 |
| | $A^0$ | 45 | 30 |

Table 3.6: This table corresponds to figure 3.11 displaying the various parameters of excitons and trions in $MoSe_2$ and heterostructure

### 3.3.3 $MoSe_2$ on gold substrate

Following the heterostructure formed by $MoSe_2$ with $TaS_2$, we fabricated a vertical van der Waals interface by transferring a monolayer of $MoSe_2$ on the clean surface of Au. To compare, we measured the PL intensity of $MoSe_2$ on PDMS before transferring to Au. After performing the PL measurements on Au, the results are analyzed in figure 3.11 c which shows the overall significant PL suppression and enhancement in positive trions formed at the interface of $MoSe_2$ and Au. As this is demonstrated in table 3.7 $A^+$ contribution to the total PL emission is increasing from 0.52 to 0.58 while the contribution from $A^0$ is decreasing from

0.48 to 0.42 validating the charge transfer happening at the interface of $MoSe_2$ and Au. Figure 3.11 a shows the OM image of a transferred $MoSe_2$ crystal on Au while figure 3.11 b shows the uniform PL map [17, 29, 86, 87].

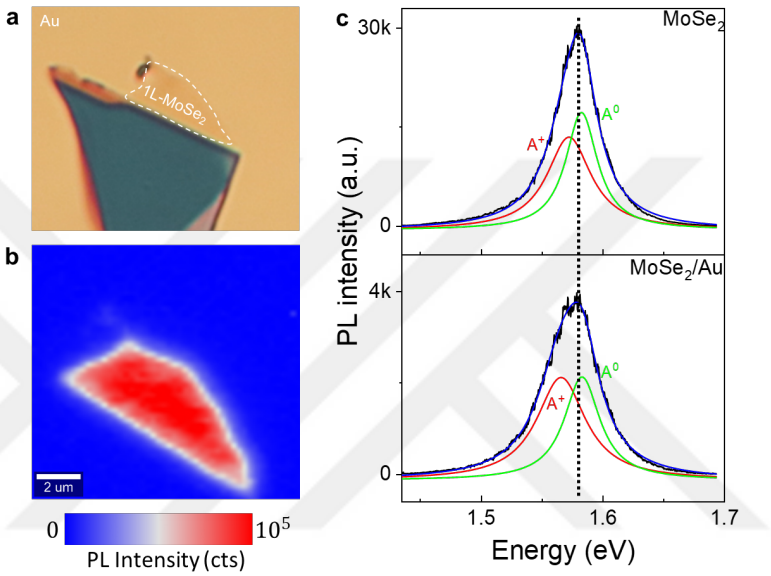


Figure 3.11: (a) OM image of $MoSe_2$ placed on top of Au substrate (b) PL map (c) PL point spectrum from $MoSe_2$ on PDMS and Au showing the huge suppression in PL intensity of MoSe2/Au

| | | $MoSe_2$ | $MoSe_2$/Au |
|---|---|---|---|
| Peak Position(eV) | $A^+$ | 1.57276 | 1.56622 |
| | $A^0$ | 1.58305 | 1.58346 |
| $Area/A_{tot}$ | $A^+$ | 0.52 | 0.58 |
| | $A^0$ | 0.48 | 0.42 |
| FWHM (meV) | $A^+$ | 44 | 49 |
| | $A^0$ | 32 | 36 |

Table 3.7: This table corresponds to figure 3.12 and shows the quantitative analysis of excitons and trions present in $MoSe_2$

## 3.4 Raman spectroscopy of $MoS_2$ on various substrates

Raman spectroscopy is a powerful, and nondestructive characterization technique for most of the materials as explained in methods. Here we will show Raman spectroscopic characterization of $MoS_2$(1L) and its heterostructure with $TaS_2$ on various substrates. $MoS_2$ has several Raman active modes such as $E^2{}_{2g}$ (32 $cm^{-1}$), $E_{1g}$ (286$cm^{-1}$), $E^1{}_{2g}$ (383 $cm^{-1}$), and $A_{1g}$ (408 $cm^{-1}$) in its bulk form. And most prominent are $A_{1g}$ (out of plane) and $E^1{}_{2g}$ (in plane) which are utilized to allocate the layer number to thin crystals as well as to show any changes at the interface of $MoS_2$ with other materials.

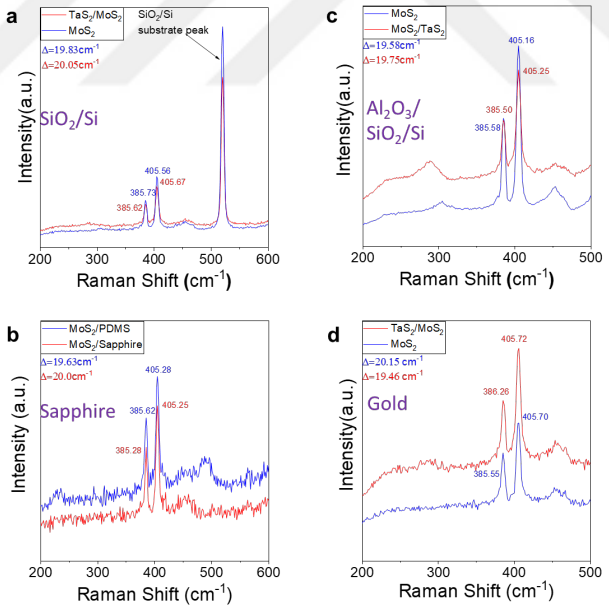


Figure 3.12: (a) Raman single spectrum from both $MoS_2$ and $TaS_2/MoS_2$ heterostructure on $SiO_2/Si$ substrate showing the small broadening in the peaks at interface (b) Raman single spectrum from both $MoS_2$ and $MoS_2/TaS_2$ heterostructure on 30 nm alumina coated $SiO_2/Si$ substrate showing the small broadening in the peaks at interface (c) Raman single spectrum from $MoS_2$ on PDMS and sapphire showing the small broadening in the peaks when $MoS_2$ is placed on sapphire (d) Raman single spectrum from both $MoS_2$ and $MoS_2/TaS_2$ heterostructure on 100 nm gold coated $SiO_2/Si$ substrate showing the small broadening in the peaks at interface

If the difference in frequency of $A_{1g}$ and $E^1{}_{2g}$ is less than 20 $cm^{-1}$, it is clear evidence that the crystal of $MoS_2$ is a monolayer. The in-plane ($E^1{}_{2g}$) mode is strain sensitive and shows some shift in the peak if some strain is applied or induced to $MoS_2$ due to heterostructure formation or interlayer coupling. As it can be seen from figure 3.10 the difference in frequency between in-plane and out-of-plane Raman modes is less than 20 $cm^{-1}$ for bare $MoS_2$ and slightly higher in heterostructure which can be due to charge transfer, strain induced at the interface due to lattice mismatch between $MoS_2$ and $TaS_2$ or the presence of $A_{1g}$ (405 $cm^{-1}$) mode of $TaS_2$. Raman spectra obtained from various substrates show difference in the peak positions but all of them are quite close which shows that there is not any drastic change except the substrate effect or interface charge transfer [80, 88, 89, 90, 91, 92].

## 3.5 Conclusion

In this chapter, we introduced and explained a novel method to control the optical properties of Mo-based TMDCs. We explained both the enhancement and suppression of PL intensity of both $MoS_2$ and $MoSe_2$. It can be inferred from the results demonstrated in section 3.2.1 that regardless of the configuration and geometry of heterostructures, PL intensity can be enhanced by hole injection to $MoS_2$ from high work function metals and maintaining van der Waals gap between the metals and $MoS_2$ crystals. Van der Waals gap is a key parameter to control the nature of charge transfer. Otherwise, electrons can easily flow to TMDCs if there is no van der Waals gap between the TMDCs and metals. In section 3.3, PL suppression of $MoS_2$ and $MoSe_2$ is presented which is also based on the same scientific argument as the enhancement. If a low work function metal is brought in contact with TMDCs, then metal provides electrons that alter the optical properties of TMDCs as in the case of $MoS_2$/Gr interface, PL is greatly reduced. For the case of $MoSe_2$, which can behave as a bipolar material, we showed that positive trions are formed because of p-type doping to $MoSe_2$ from both $TaS_2$ and Au.

# Chapter 4

# Vertical heterostructures of tungsten-based chalcogenides with 2D/3D metals

## 4.1 Introduction

Tungsten disulfide ($WS_2$) and Tungsten diselenide ($WSe_2$) are also well-studied 2D TMDCs after $MoS_2$. $WS_2$ is a high band gap semiconductor and increases even more when it is thinned down to a monolayer due to the transition in the gap from indirect to direct [30, 31]. $WSe_2$ is a smaller gap semiconductor (1.64 eV for 1L) as compared to $WS_2$ (2.1 eV) though it has the same transition in the gap as $WS_2$ [27, 31]. One interesting difference between these two materials is the nature of carrier transport. $WS_2$ usually behaves as n-type [37, 93, 94] and $WSe_2$ shows the ambipolar response in the transfer curve obtained from gating measurements [41, 42, 45]. This difference in the nature of these materials makes them good candidates for tuning their optical properties. In this chapter, we investigated the effect of doping (both n-type and p-type) on the photoluminescence of these materials by strategically fabricating the heterostructures with various 2D/3D metals and utilizing the van der Waals gap.

## 4.2 PL enhancement

In this section, we will explain PL enhancement in tungsten-based TMDC heterostructures with metals. We carefully fabricated heterostructures of $WS_2$ and various high work function metals such as $TaS_2$, Au, and Pt to observe the PL enhancement. To show the significance of the van der Waals gap in these heterostructures, we annealed our sample fabricated on Au substrate. We did PL, Raman, and XPS measurements after annealing to demonstrate that the van der Waals gap is compulsory for PL enhancement.

### 4.2.1 $WS_2$ and $TaS_2$ heterostructures

$TaS_2$ is a 2D metallic material having a higher work function of ($\approx 5.6eV$) [61] which makes it a good p-type dopant since the Schottky barrier height for holes decreases with increasing work function according to Schottky Mott law. We fabricated the heterostructures using standard exfoliation and dry transfer techniques mentioned in detail in the methods. We placed a few layered $TaS_2$ partially on top of the $WS_2$ monolayer to see the difference in the PL intensity of $WS_2$ bare and under $TaS_2$ which was optically transparent. As expected, we observed the enhancement in the PL intensity of the heterostructure. Since $WS_2$ is an n-type material, upon interfacing with $TaS_2$ which transfers holes to the valence band of $WS_2$ and reduces the number of trions ($A^-$) which are formed due to extra electrons present in $WS_2$. The enhancement in the PL intensity at the interface is obvious in figures 4.1 b and c which show the PL maps and point spectrum. This is also well explained in table 4.1 which shows the quantitative analysis of trions and excitons. Peaks for both the excitons and trions are shifting in the heterostructure towards higher energy indicating an increased number of excitonic recombinations which is also obvious in the areal ratio (obtained by dividing the area of trion or exciton to the total area obtained from Lorentzian fitting through Origin) [1, 17, 19, 27, 30, 31, 94].

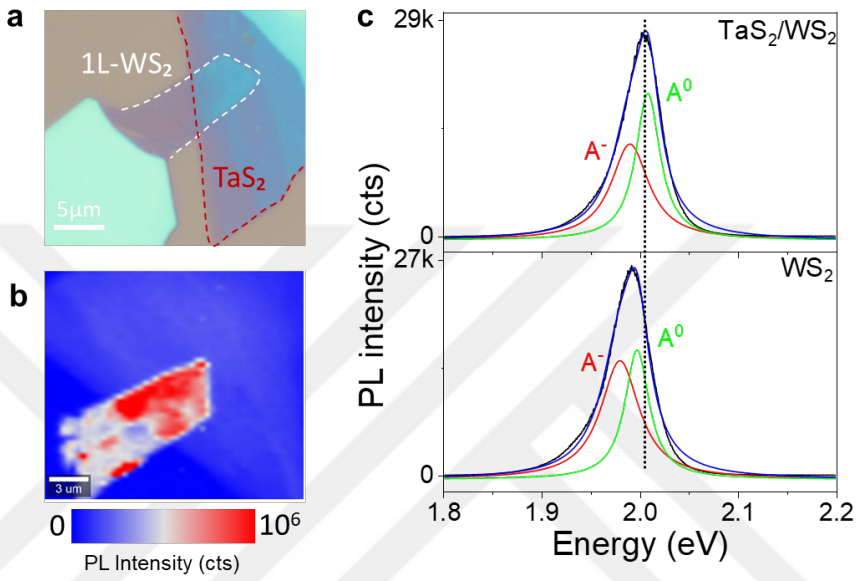


Figure 4.1: (a) OM image of hetero-structure with $TaS_2$ on top of $WS_2$ on 300 nm coated $SiO_2$/Si substrate(b) PL Map (c) PL point spectrum $WS_2$ and hetero-structure

| | | $WS_2$ | $TaS_2/WS_2$ |
|---|---|---|---|
| Peak Position(eV) | $A^-$ | 1.98 | 1.99013 |
| | $A^0$ | 1.99736 | 2.00836 |
| $Area/A_{tot}$ | $A^-$ | 0.5935 | 0.5024 |
| | $A^0$ | 0.4065 | 0.4976 |
| FWHM (meV) | $A^-$ | 48 | 47 |
| | $A^0$ | 30 | 30 |

Table 4.1: This table corresponds to figure 4.1 and showing the quantitative data obtained via Lorentzian fitting

### 4.2.2 $WS_2$ and gold heterostructures

#### 4.2.2.1 PL measurements of $WS_2$ on gold before and after annealing

In this section, we demonstrated the impact of the van der Waals gap in these heterostructures. After obtaining a suitable crystal by mechanical exfoliation of $WS_2$ on the PDMS stamp, we performed PL measurements on PDMS to have a comparison with Au. We observed a drastic enhancement in the PL intensity of $WS_2$ on Au because of p-type doping and van der Waals gap between the $WS_2$ and Au surface as it is obvious in figure 4.2 b and e. Figure 4.2 b shows the uniform PL map of $WS_2$ crystal before annealing and figure 4.2 e shows the point spectrum of $WS_2$ on PDMS as well as on Au before and after annealing. Table 4.2 also demonstrates the quantitative analysis of $A^0$, $A^-$. The spectral weight of $A^-$ is 0.33 on PDMS which reduces to 0.09 when $WS_2$ is transferred onto Au substrate indicating the strong charge transfer at the interface.

Moreover, we annealed our sample using a CVD furnace by increasing the temperature very slowly from room temperature to 580 K under inert Ar flow and kept the sample at 580 K for 15 minutes before cooling down. After annealing, there are not any excitonic recombinations as well as almost vanished PL intensity in $WS_2$ showing the significance of the van der Waals gap. Photocarriers from $WS_2$ are easily transferred to Au after excitation with a laser if there is no van der Waals gap. We also observed the same behavior in another $WS_2$ sample to ensure the reproducibility and reliability of these observations. In addition to PL quenching of $WS_2$ after annealing, the physical appearance of the monolayered part is also different than before annealing as shown in figures 4.2 a, and c. The Intensity in the PL map also drastically drops down after annealing [1, 17, 19, 27, 30, 31, 94]. This section explains the importance of the van der Waals gap and based on these observations we can say that we will obtain the same results if we anneal all other samples.

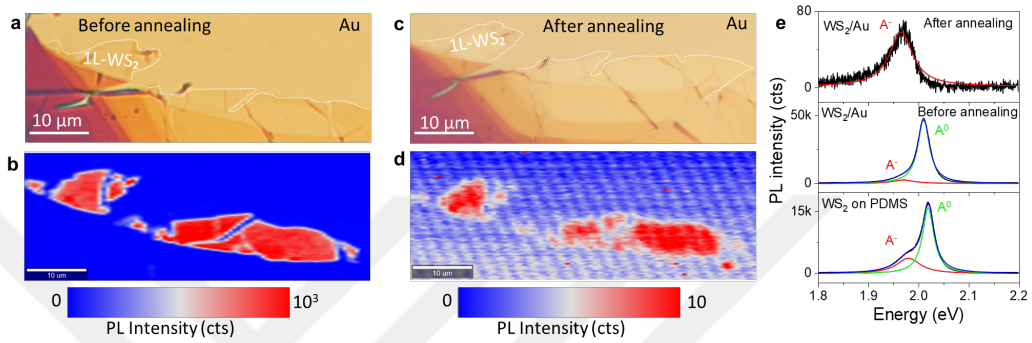


Figure 4.2: (a) OM image of $WS_2$ transferred on top of 100 nm gold coated $SiO_2$/Si substrate before annealing(b) PL map before annealing (c) OM image of $WS_2$ transferred on top of 100 nm gold coated $SiO_2$/Si substrate after annealing indicating a clear difference in optical contrast which can be an evidence for no van der Waals gap (d) PL map after annealing (e) PL point spectrum on PDMS and gold (before and after annealing)

| | | $WS_2$/PDMS | Before annealing | After annealing |
|---|---|---|---|---|
| Peak Position (eV) | $A^-$ | 1.98036 | 1.97936 | 1.97847 |
| | $A^0$ | 2.01961 | 2.018932 | N/A |
| $Area/A_{tot}$ | $A^-$ | 0.33 | 0.09 | 1 |
| | $A^0$ | 0.67 | 0.91 | N/A |
| FWHM (meV) | $A^-$ | 58 | 52 | 60 |
| | $A^0$ | 27 | 27 | N/A |

Table 4.2: This table corresponds to figure 4.2 and shows the quantitative data obtained via Lorentzian fitting of PL data.

#### 4.2.2.2 XPS measurements before and after annealing

X-ray photo electron spectroscopy (XPS) serves as a valuable surface-sensitive technique for elemental identification within materials, operating on the fundamental principles of the photoelectric effect. In this characterization technique, X-rays are directed onto the sample, inducing the emission of electrons. These emitted electrons are subsequently captured by a detector, which is connected to the software and plots binding energy vs counts of electrons.

In addition to elemental identification, XPS can also be useful to observe any chemical or electronic spectral changes to the surface of any material. Since, annealing changes the bonding and electronic spectra of the interface of $WS_2$, and Au we did XPS measurements before and after annealing to validate the claim that after annealing we do not have any van der Waals gap between $WS_2$ and Au surface. The shift in peak positions of W (4f), and S (2p) orbitals towards lower binding energy suggests that the electronic spectra has been changed due to no gap between Au and $WS_2$ [95, 96, 97, 98].

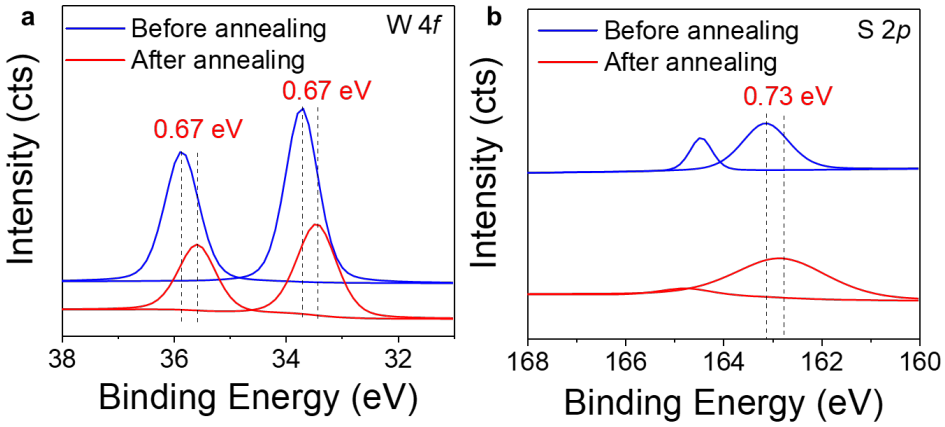


Figure 4.3: (a) 4f orbital of W before and after annealing indicating a redshift in binding energy (b) 2p orbital of S before and after annealing indicating a redshift in binding energy

### 4.2.3 $WS_2$ and platinum heterostructures

Platinum (Pt) is also a high work function (5.6 eV) noble metal. We deposited a 30 nm layer of Pt using a precision etching coating system (PECS) on top of $SiO_2$/Si substrate and transferred a monolayer of $WS_2$ on top of it. To give another evidence of p-type doping because of the high work function of Pt and van der Waals gap in between $WS_2$ and Pt surface. PL intensity was also increased in this interface giving another strong evidence to our claim of universal control of PL of TMDCs. As it is obvious in figures 4.4 b, c, and table 4.3 that there was a huge enhancement in the PL, and no trion peak was observed at all when we tried to fit the data using Lorentzian fitting. The 4-fold enhancement in PL, disappearing trionic peak, and blue shift to the excitonic peak position strongly suggest the p-type doping from Pt to $WS_2$. Pt has already been studied and shown the better p-type doping to $MoS_2$ and we also confirm it here using $WS_2$ [1, 17, 19, 27, 30, 31, 94].

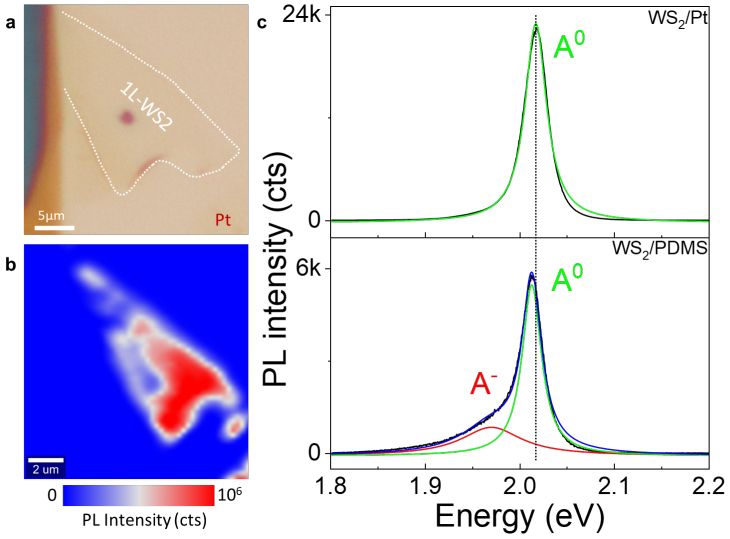


Figure 4.4: (a) OM image of $WS_2$ transferred on top of 30 nm Pt coated $SiO_2$/Si substrate (b) PL map (c) PL point spectrum showing the comparison between $WS_2$-1L on PDMS and Pt

| | | $WS_2$/PDMS | $WS_2$/Pt |
|---|---|---|---|
| Peak Position(eV) | $A^-$ | 1.97033 | N/A |
| | $A^0$ | 2.01303 | 2.01729 |
| Area/$A_{tot}$ | $A^-$ | 0.34 | N/A |
| | $A^0$ | 0.66 | 1 |
| FWHM (meV) | $A^-$ | 78 | N/A |
| | $A^0$ | 25 | 28 |

Table 4.3: This table corresponds to figure 4.3 and showing the quantitative data obtained via Lorentzian fitting of PL point spectrum plotted in figure 4.3 c

## 4.3 Photoluminescence suppression

### 4.3.1 $WS_2$ and silver heterostructure

Silver (Ag) is known for its best electron doping capability to semiconductors because of its low work function (4.3 eV). Schottky barrier height for electrons is very small when Ag is interfaced with TMDCs. We transferred a single layer of $WS_2$ on top of Ag and did the PL measurements, before and after transferring. We observed a huge suppression in PL and enhancement in the number of trions, which indicates that $WS_2$ is receiving electrons from Ag and hence reduction in the excitons, and ultimately the suppression in the overall PL emission intensity as shown in figure 4.5 and table 4.4. The suppression in the PL intensity, red-shift in peak positions of $A^0$, and $A^-$, suppression in spectral weight of $A^0$, and enlargement in spectral weight of $A^-$ indicate that there is strong n-type doping to $WS_2$ from Ag [1, 17, 19, 27, 30, 31, 94]..

| | | $WS_2$/PDMS | $WS_2$/Ag |
|---|---|---|---|
| Peak Position(eV) | $A^-$ | 1.98706 | 1.99396 |
| | $A^0$ | 2.02167 | 2.0094 |
| Area/$A_{tot}$ | $A^-$ | 0.22 | 0.46 |
| | $A^0$ | 0.78 | 0.54 |
| FWHM (meV) | $A^-$ | 66 | 40 |
| | $A^0$ | 25 | 26 |

Table 4.4: This table corresponds to figure 4.5 showing the quantitative data obtained via Lorentzian fitting of PL point spectrum plotted in figure 4.5 c

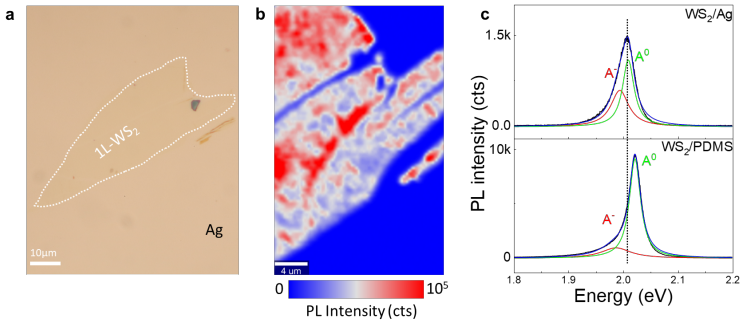


Figure 4.5: (a) OM image of $WS_2$ transferred on top of 30 nm Ag coated $SiO_2$/Si substrate (b) PL map (c) PL point spectrum showing the comparison between $WS_2$-1L on PDMS and Ag

## 4.4 $WSe_2$ and $TaS_2$ heterostructures

$WSe_2$ is an ambipolar semiconducting material and shows the direct transition of charge carriers when it is thinned down to a monolayer. Depending on the nature of the interfaced material, its PL intensity can be manipulated with the negative and positive charge injection. If a heterostructure is formed between a metal and $WSe_2$, it can dope $WSe_2$ with either holes or electrons depending on the work function of the metal.

$TaS_2$ can be used as a hole dopant to semiconducting materials, and we exploited its ability to donate holes to $WSe_2$ in this section. Since $WSe_2$ prefers p-type behavior, its PL can be reduced by adding more holes into it due to the formation of positive trions ($A^+$). We experimented and confirmed that the PL intensity of $MoSe_2$ can be reduced upon p-type doping by $TaS_2$. Moreover, van der Waals gap is also compulsory for this charge injection. As explained in section 4.2.1, if there is no Van der Waals gap in these heterostructures, we will get a huge suppression of PL. It is shown in figure 4.6 b that PL is reduced significantly at the interface of $WSe_2$ and $TaS_2$, and we got a positive trion due to hole injection from $TaS_2$ as well at the interface [1, 5, 19, 41, 42, 45, 46, 47].

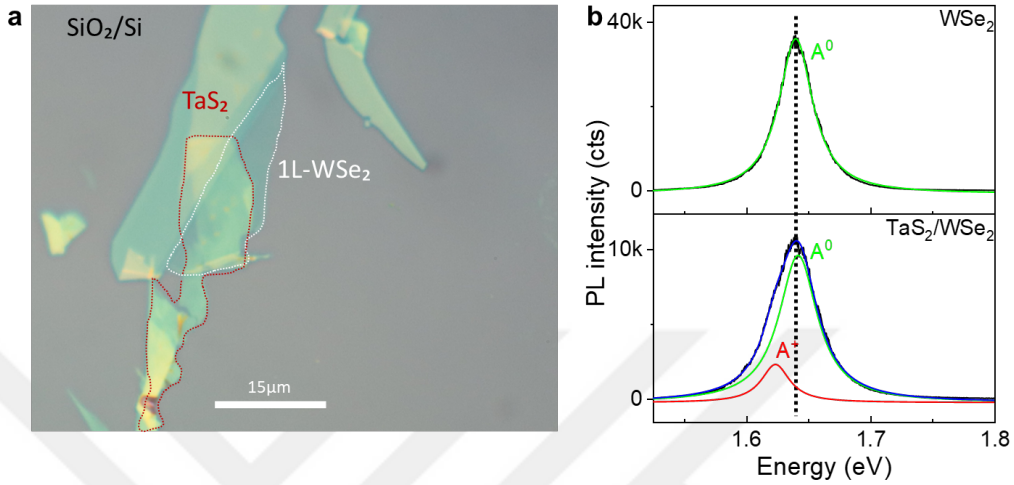


Figure 4.6: (a) OM image of $TaS_2$ placed on top of $WSe_2$ on $SiO_2$/Si substrate (b) PL point spectrum from bare $WSe_2$ and hetero-structure showing the huge suppression in PL intensity at interface and the appearance of positive trions at interface

| | | $WSe_2$ | $TaS_2/WSe_2$ |
|---|---|---|---|
| Peak Position(eV) | $A^+$ | N/A | 1.6236 |
| | $A^0$ | 1.63996 | 1.64188 |
| $Area/A_{tot}$ | $A^+$ | N/A | 0.16 |
| | $A^0$ | 1 | 0.84 |
| FWHM (meV) | $A^+$ | N/A | 28 |
| | $A^0$ | 33 | 37 |

Table 4.5: This table corresponds to figure 4.6.

## 4.5 Conclusion

In this chapter, we successfully managed to enhance and suppress the PL intensity of $WS_2$ and $WSe_2$ by making van der Waals heterostructures of $WS_2$ and $WSe_2$ with 2D/3D metals such as $TaS_2$, Au, Pt, and Ag utilizing the work function of metals. Moreover, We investigated the significance of the van der Waals gap between these heterojunctions. PL and XPS measurements before and after annealing show the importance of the van der Waals gap. We systematically explored the tunability of PL intensity of $WS_2$ and $WSe_2$ by using different work

function metals to inject different charge carriers to $WS_2$ and $WSe_2$. Our results offer a comprehensive way to control the fundamental optical properties of TMDCs which can be utilized in LEDs, lasers, and other optoelectronic devices.

# Chapter 5

# Conclusion and Future Works

Metal semiconductor interfaces are of huge importance in terms of nanoelectronics and have been explored quite extensively in the community of 2D materials and there are many thorough studies devoted to these interfaces exploring transport properties and their various parameters. In this study, we investigated the optical properties of semiconducting TMDCs when interfaced with 2D/3D metals and our observations offer a universal way to control the PL intensity of these TMDCs. In our study, we successfully tested various metal-semiconductor heterostructures fabricated with different 2D/3D metals such as $TaS_2$, $NbTe_2$, graphene, Ag, Au, and Pt with $MoS_2$, $WS_2$, $WSe_2$, and $MoSe_2$. We showed in this study that the type of charge carrier injection depends on the work function of metal if there is a van der Waals gap between metal and semiconductor. A higher work function metal has lower SBH for holes and hence dopes semiconductors with a positive charge and influences the optical properties of these TMDCs. If an n-type TMDC material like $MoS_2$, then its PL intensity is enhanced significantly and the shape of the peak also gets better because free electrons are reduced and so are the defects. If the nature of the TMDC is p-type, like $WSe_2$, and is interfaced with a higher work function metal that gives more holes to $WSe_2$ ending up with more positive trions and reduction in PL intensity.

In addition to room temperature measurements, we also performed

temperature-dependent PL measurements of $TaS_2/MoS_2$ heterostructures on $SiO_2$/Si and Au substrates. The temperature-dependent PL measurements on $SiO_2$/Si substrate show persistent biexcitons throughout all the temperatures while on Au, they can only be observed at lower temperatures due to the substrate effect and thin film interference as well as higher work function of Au. Biexcitons observed in $SiO_2$/Si substrate start converting into trions or excitons after 250 K which has not been reported before.

We also performed PL measurements under an external electric field and observed very peculiar results that had not been reported before. PL measurements under the external field for bare $MoS_2$ were the same as already observed by various groups and reported in several reports. However, at the interface of $TaS_2/MoS_2$ we observed persistent exciton even when the applied back gate voltage was 100 V. The possible reason behind this could be the continuous hole injection from $TaS_2$ to $MoS_2$ at the interface.

Moreover, we also investigated the significance of the van der Waals gap by performing PL and XPS measurements before and after annealing. PL intensity almost vanishes after annealing while a drop of 0.67 eV and 0.73 eV in the binding energy of 4f and 2p orbitals of W and S respectively. These results further validate the elimination and consequences of the elimination of van der Waals gap.

| | $MoS_2$ | $MoSe_2$ | $WS_2$ | $WSe_2$ |
|---|---|---|---|---|
| $TaS_2$ | 7 | 0.2 | 1.08 | 0.32 |
| $NbTe_2$ | 1.6 | - | - | - |
| Graphene | 0.24 | - | - | - |
| Au | 1.4 | 0.13 | 3.1 | - |
| Pt | - | - | 3.7 | - |
| Ag | - | - | 0.2 | - |

Table 5.1: This table shows the enhancement factor of PL intensity in various interfaces. The first column shows 2D/3D metals and the first row shows TMDCs we used in this study. Blue colored numbers are showing the enhancement and red colored numbers are showing the quenching factor.

To sum up, This work shows a universal way to control the PL intensity utilizing the van der Waals gap and metal work function as illustrated in the

table that we can enhance or suppress the PL intensity of TMDCs by carefully choosing the metal and TMDC material. These observations provide a platform for novel optoelectronic devices, LEDs, and lasers.

# Bibliography


[1] Y. Liu, J. Guo, E. Zhu, L. Liao, S.-J. Lee, M. Ding, I. Shakir, V. Gambin, Y. Huang, and X. Duan, "Approaching the schottky–mott limit in van der waals metal–semiconductor junctions," *Nature*, vol. 557, no. 7707, pp. 696–700, 2018.

[2] K. S. Novoselov, A. K. Geim, S. V. Morozov, D.-e. Jiang, Y. Zhang, S. V. Dubonos, I. V. Grigorieva, and A. A. Firsov, "Electric field effect in atomically thin carbon films," *science*, vol. 306, no. 5696, pp. 666–669, 2004.

[3] Y. Li, C. Y. Xu, J. K. Qin, W. Feng, J. Y. Wang, S. Zhang, L. P. Ma, J. Cao, P. A. Hu, W. Ren, and L. Zhen, "Tuning the Excitonic States in MoS2/Graphene van der Waals Heterostructures via Electrochemical Gating," *Advanced Functional Materials*, vol. 26, no. 2, pp. 293–302, 2016.

[4] R. Ganatra and Q. Zhang, "Few-layer MoS2: A promising layered semiconductor," *ACS Nano*, vol. 8, no. 5, pp. 4074–4099, 2014.

[5] L. Wang, X. Xu, L. Zhang, R. Qiao, M. Wu, Z. Wang, S. Zhang, J. Liang, Z. Zhang, Z. Zhang, W. Chen, X. Xie, J. Zong, Y. Shan, Y. Guo, M. Willinger, H. Wu, Q. Li, W. Wang, P. Gao, S. Wu, Y. Zhang, Y. Jiang, D. Yu, E. Wang, X. Bai, Z. J. Wang, F. Ding, and K. Liu, "Epitaxial growth of a 100-square-centimetre single-crystal hexagonal boron nitride monolayer on copper," *Nature*, vol. 570, no. 7759, pp. 91–95, 2019.

[6] Z. Cai, B. Liu, X. Zou, and H. M. Cheng, "Chemical Vapor Deposition Growth and Applications of Two-Dimensional Materials and Their Heterostructures," *Chemical Reviews*, vol. 118, no. 13, pp. 6091–6133, 2018.

[7] T. Knobloch, Y. Y. Illarionov, F. Ducry, C. Schleich, S. Wachter, K. Watanabe, T. Taniguchi, T. Mueller, M. Waltl, M. Lanza, M. I. Vexler, M. Luisier, and T. Grasser, "The performance limits of hexagonal boron nitride as an insulator for scaled CMOS devices based on two-dimensional materials," *Nature Electronics*, vol. 4, no. 2, pp. 98–108, 2021.

[8] K. S. Novoselov, D. Jiang, F. Schedin, T. J. Booth, V. V. Khotkevich, S. V. Morozov, and A. K. Geim, "Two-dimensional atomic crystals," *Proceedings of the National Academy of Sciences of the United States of America*, vol. 102, no. 30, pp. 10451–10453, 2005.

[9] A. K. Geim and K. S. Novoselov, "The rise of graphene PROGRESS," *Nature Materials*, vol. 6, no. 3, pp. 183–191, 2007.

[10] A. K. Geim, "Graphene: Status and prospects," *Science*, vol. 324, no. 5934, pp. 1530–1534, 2009.

[11] M. Yi and Z. Shen, "A review on mechanical exfoliation for the scalable production of graphene," *Journal of Materials Chemistry A*, vol. 3, no. 22, pp. 11700–11715, 2015.

[12] P. C. Shen, Y. Lin, H. Wang, J. H. Park, W. S. Leong, A. Y. Lu, T. Palacios, and J. Kong, "CVD Technology for 2-D Materials," *IEEE Transactions on Electron Devices*, vol. 65, no. 10, pp. 4040–4052, 2018.

[13] M. Chhowalla, Z. Liu, and H. Zhang, "Two-dimensional transition metal dichalcogenide (TMD) nanosheets," *Chemical Society Reviews*, vol. 44, no. 9, pp. 2584–2586, 2015.

[14] H. Zhang, M. Chhowalla, and Z. Liu, "2D nanomaterials: Graphene and transition metal dichalcogenides," *Chemical Society Reviews*, vol. 47, no. 9, pp. 3015–3017, 2018.

[15] X. Lin, P. Yan, F. Xu, W. Wu, T. Hu, C. Wei, and Q. Xu, "Solid-phase synthesis of atomically thin two-dimensional non-layered MoO2 nanosheets for surface enhanced Raman spectroscopy," *Journal of Materials Chemistry C*, vol. 7, no. 24, pp. 7196–7200, 2019.

[16] B. Zhao, D. Shen, Z. Zhang, P. Lu, M. Hossain, J. Li, B. Li, and X. Duan, "2D Metallic Transition-Metal Dichalcogenides: Structures, Synthesis, Properties, and Applications," *Advanced Functional Materials*, vol. 31, no. 48, pp. 1–36, 2021.

[17] W. Chen, C. Zheng, J. Pei, and H. Zhan, "External field regulation strategies for exciton dynamics in 2D TMDs," *Optical Materials Express*, vol. 13, no. 4, p. 1007, 2023.

[18] L. Stojchevska, I. Vaskivskyi, T. Mertelj, P. Kusar, D. Svetin, S. Brazovskii, and D. Mihailovic, "Ultrafast switching to a stable hidden quantum state in an electronic crystal," *Science*, vol. 344, no. 6180, pp. 177–180, 2014.

[19] Y. Liu, P. Stradins, and S. H. Wei, "Van der Waals metal-semiconductor junction: Weak Fermi level pinning enables effective tuning of Schottky barrier," *Science Advances*, vol. 2, no. 4, pp. 1–7, 2016.

[20] J. A. Del Alamo, "Nanometre-scale electronics with III-V compound semiconductors," *Nature*, vol. 479, no. 7373, pp. 317–323, 2011.

[21] H. H. Huang, X. Fan, D. J. Singh, and W. T. Zheng, "Recent progress of TMD nanomaterials: Phase transitions and applications," *Nanoscale*, vol. 12, no. 3, pp. 1247–1268, 2020.

[22] R. Wang, Y. Yu, S. Zhou, H. Li, H. Wong, Z. Luo, L. Gan, and T. Zhai, "Strategies on Phase Control in Transition Metal Dichalcogenides," *Advanced Functional Materials*, vol. 28, no. 47, pp. 1–17, 2018.

[23] O. Samy, S. Zeng, M. D. Birowosuto, and A. El Moutaouakil, "A review on mos2 properties, synthesis, sensing applications and challenges," *Crystals*, vol. 11, no. 4, 2021.

[24] Z. He and W. Que, "Molybdenum disulfide nanomaterials: Structures, properties, synthesis and recent progress on hydrogen evolution reaction," *Applied Materials Today*, vol. 3, pp. 23–56, 2016.

[25] J. Strachan, A. F. Masters, and T. Maschmeyer, "3R-MoS2in Review: History, Status, and Outlook," *ACS Applied Energy Materials*, vol. 4, no. 8, pp. 7405–7418, 2021.

[26] L. Cai, W. Cheng, T. Yao, Y. Huang, F. Tang, Q. Liu, W. Liu, Z. Sun, F. Hu, Y. Jiang, W. Yan, and S. Wei, "High-content metallic 1t phase in mos2-based electrocatalyst for efficient hydrogen evolution," *The Journal of Physical Chemistry C*, vol. 121, no. 28, pp. 15071–15077, 2017.

[27] M. Farmanbar and G. Brocks, "Ohmic Contacts to 2D Semiconductors through van der Waals Bonding," *Advanced Electronic Materials*, vol. 2, no. 4, pp. 2–9, 2016.

[28] J. K. Ellis, M. J. Lucero, and G. E. Scuseria, "The indirect to direct band gap transition in multilayered MoS 2 as predicted by screened hybrid density functional theory," *Applied Physics Letters*, vol. 99, no. 26, 2011.

[29] Y. Zhang, T. R. Chang, B. Zhou, Y. T. Cui, H. Yan, Z. Liu, F. Schmitt, J. Lee, R. Moore, Y. Chen, H. Lin, H. T. Jeng, S. K. Mo, Z. Hussain, A. Bansil, and Z. X. Shen, "Direct observation of the transition from indirect to direct bandgap in atomically thin epitaxial MoSe2," *Nature Nanotechnology*, vol. 9, no. 2, pp. 111–115, 2014.

[30] Y. Ma, Y. Dai, M. Guo, C. Niu, J. Lu, and B. Huang, "Electronic and magnetic properties of perfect, vacancy-doped, and nonmetal adsorbed MoSe2, MoTe2 and WS2 monolayers," *Physical Chemistry Chemical Physics*, vol. 13, no. 34, pp. 15546–15553, 2011.

[31] H. R. Gutiérrez, N. Perea-López, A. L. Elías, A. Berkdemir, B. Wang, R. Lv, F. López-Urías, V. H. Crespi, H. Terrones, and M. Terrones, "Extraordinary room-temperature photoluminescence in triangular WS 2 monolayers," *Nano Letters*, vol. 13, no. 8, pp. 3447–3454, 2013.

[32] K. N. Shinde, S. J. Dhoble, H. C. Swart, and K. Park, *Basic Mechanisms of Photoluminescence*, pp. 41–59. Berlin, Heidelberg: Springer Berlin Heidelberg, 2012.

[33] H. B. Bebb and E. W. Williams, "Photoluminescence I: Theory," *Semiconductors and Semimetals*, vol. 8, no. C, pp. 181–320, 1972.

[34] S. A. Empedocles, R. Neuhauser, K. Shimizu, and M. G. Bawendi, "Photoluminescence from single semiconductor nanostructures," *Advanced Materials*, vol. 11, no. 15, pp. 1243–1256, 1999.

[35] K. F. Mak, K. He, C. Lee, G. H. Lee, J. Hone, T. F. Heinz, and J. Shan, "Tightly bound trions in monolayer MoS 2," *Nature Materials*, vol. 12, no. 3, pp. 207–211, 2013.

[36] Y. Lin, X. Ling, L. Yu, S. Huang, A. L. Hsu, Y. H. Lee, J. Kong, M. S. Dresselhaus, and T. Palacios, "Dielectric screening of excitons and trions in single-layer MoS2," *Nano Letters*, vol. 14, no. 10, pp. 5569–5576, 2014.

[37] A. Sebastian, R. Pendurthi, T. H. Choudhury, J. M. Redwing, and S. Das, "Benchmarking monolayer MoS2 and WS2 field-effect transistors," *Nature Communications*, vol. 12, no. 1, pp. 1–12, 2021.

[38] M. Amani, D. H. Lien, D. Kiriya, J. Xiao, A. Azcatl, J. Noh, S. R. Madhvapathy, R. Addou, K. C. Santosh, M. Dubey, K. Cho, R. M. Wallace, S. C. Lee, J. H. He, J. W. Ager, X. Zhang, E. Yablonovitch, and A. Javey, "Near-unity photoluminescence quantum yield in MoS2," *Science*, vol. 350, no. 6264, pp. 1065–1068, 2015.

[39] H. Nan, Z. Wang, W. Wang, Z. Liang, Y. Lu, Q. Chen, D. He, P. Tan, F. Miao, X. Wang, J. Wang, and Z. Ni, "Strong photoluminescence enhancement of MoS2 through defect engineering and oxygen bonding," *ACS Nano*, vol. 8, no. 6, pp. 5738–5745, 2014.

[40] M. Ramos, F. Marques-Moros, D. L. Esteras, S. Mañas-Valero, E. Henríquez-Guerra, M. Gadea, J. J. Baldoví, J. Canet-Ferrer, E. Coronado, and M. R. Calvo, "Photoluminescence Enhancement by Band Alignment Engineering in MoS2/FePS3van der Waals Heterostructures," *ACS Applied Materials and Interfaces*, 2022.

[41] H. Wu, Z. Yan, Z. Xie, and S. Zhu, "WSe2/Pd Schottky diode combining van der Waals integrated and evaporated metal contacts," *Applied Physics Letters*, vol. 119, no. 21, 2021.

[42] J. Jang, H. S. Ra, J. Ahn, T. W. Kim, S. H. Song, S. Park, T. Taniguch, K. Watanabe, K. Lee, and D. K. Hwang, "Fermi-Level Pinning-Free WSe2 Transistors via 2D Van der Waals Metal Contacts and Their Circuits," *Advanced Materials*, vol. 34, no. 19, pp. 1–8, 2022.

[43] G. Kwon, Y. H. Choi, H. Lee, H. S. Kim, J. Jeong, K. Jeong, M. Baik, H. Kwon, J. Ahn, E. Lee, and M. H. Cho, "Interaction- and defect-free van der Waals contacts between metals and two-dimensional semiconductors," *Nature Electronics*, vol. 5, no. 4, pp. 241–247, 2022.

[44] Y. Wang, J. C. Kim, R. J. Wu, J. Martinez, X. Song, J. Yang, F. Zhao, A. Mkhoyan, H. Y. Jeong, and M. Chhowalla, "Van der Waals contacts between three-dimensional metals and two-dimensional semiconductors," *Nature*, vol. 568, no. 7750, pp. 70–74, 2019.

[45] Y. Sata, R. Moriya, S. Masubuchi, K. Watanabe, T. Taniguchi, and T. Machida, "N- and p-type carrier injections into WSe2 with van der Waals contacts of two-dimensional materials," *Japanese Journal of Applied Physics*, vol. 56, no. 4, pp. 4–8, 2017.

[46] K. Noori, F. Xuan, and S. Y. Quek, "Origin of contact polarity at metal-2D transition metal dichalcogenide interfaces," *npj 2D Materials and Applications*, vol. 6, no. 1, pp. 1–7, 2022.

[47] J. Kang, W. Liu, D. Sarkar, D. Jena, and K. Banerjee, "Computational study of metal contacts to monolayer transition-metal dichalcogenide semiconductors," *Physical Review X*, vol. 4, no. 3, pp. 1–14, 2014.

[48] M. Razeghi, M. Üstünçelik, F. Shabani, H. V. Demir, and T. S. Kasırga, "Plasmon-enhanced photoresponse of single silver nanowires and their network devices," *Nanoscale Horizons*, vol. 7, no. 4, pp. 396–402, 2022.

[49] M. Razeghi, J. Spiece, O. Oğuz, D. Pehlivanoğlu, Y. Huang, A. Sheraz, U. Başçı, P. S. Dobson, J. M. Weaver, P. Gehring, and T. S. Kasırga, "Single-material MoS2 thermoelectric junction enabled by substrate engineering," *npj 2D Materials and Applications*, vol. 7, no. 1, pp. 1–6, 2023.

[50] B. S. Flavel, J. G. Shapter, and J. S. Quinton, "Nanosphere lithography using thermal evaporation of gold," in *2006 International Conference on Nanoscience and Nanotechnology*, IEEE, 2006.

[51] F. H. Dill, "Optical lithography," *IEEE transactions on electron devices*, vol. 22, no. 7, pp. 440–444, 1975.

[52] B. Wu and A. Kumar, "Extreme ultraviolet lithography: A review," *Journal of Vacuum Science & Technology B: Microelectronics and Nanometer Structures Processing, Measurement, and Phenomena*, vol. 25, no. 6, pp. 1743–1761, 2007.

[53] E. Smith and G. Dent, *Modern Raman spectroscopy: a practical approach*. John Wiley & Sons, 2019.

[54] L. Andre Lyon, C. D. ine K ing, A. P. Fox, and B. E. Ba, "Raman Spect roscopy L.," *Analytical Chemistry*, vol. 2700, no. 98, pp. 341–362, 1998.

[55] S. Mouri, Y. Miyauchi, and K. Matsuda, "Tunable photoluminescence of monolayer MoS2 via chemical doping," *Nano Letters*, vol. 13, no. 12, pp. 5944–5948, 2013.

[56] R. Saito, Y. Tatsumi, S. Huang, X. Ling, and M. S. Dresselhaus, "Raman spectroscopy of transition metal dichalcogenides," *Journal of Physics Condensed Matter*, vol. 28, no. 35, 2016.

[57] P. Tonndorf, R. Schmidt, P. Böttger, X. Zhang, J. Börner, A. Liebig, M. Albrecht, C. Kloc, O. Gordan, D. R. T. Zahn, S. M. de Vasconcellos, and R. Bratschitsch, "Photoluminescence emission and raman response of monolayer mos2, mose2, and wse2," *Opt. Express*, vol. 21, pp. 4908–4916, Feb 2013.

[58] S. Haldar, H. Vovusha, M. K. Yadav, O. Eriksson, and B. Sanyal, "Systematic study of structural, electronic, and optical properties of atomic-scale defects in the two-dimensional transition metal dichalcogenides MX2 (M = Mo, W; X = S, Se, Te)," *Physical Review B - Condensed Matter and Materials Physics*, vol. 92, no. 23, pp. 1–12, 2015.

[59] J. Pandey and A. Soni, "Unraveling biexciton and excitonic excited states from defect bound states in monolayer MoS 2," *Applied Surface Science*, vol. 463, no. July 2018, pp. 52–57, 2019.

[60] T. (https://mathoverflow.net/users/84169/thomas), "Lorentzian vs gaussian fitting functions." MathOverflow. URL:https://mathoverflow.net/q/226181 (version: 2015-12-15).

[61] L. Li, J. Zhang, G. Myeong, W. Shin, H. Lim, B. Kim, S. Kim, T. Jin, S. Cavill, B. S. Kim, C. Kim, J. Lischner, A. Ferreira, and S. Cho, "Gate-Tunable Reversible Rashba-Edelstein Effect in a Few-Layer Graphene/2H-TaS2 Heterostructure at Room Temperature," *ACS Nano*, vol. 14, no. 5, pp. 5251–5259, 2020.

[62] M. Ramos, F. Marques-Moros, D. L. Esteras, S. Mañas-Valero, E. Henríquez-Guerra, M. Gadea, J. J. Baldoví, J. Canet-Ferrer, E. Coronado, and M. R. Calvo, "Photoluminescence enhancement by band alignment engineering in mos2/feps3 van der waals heterostructures," *ACS Applied Materials & Interfaces*, vol. 14, no. 29, pp. 33482–33490, 2022. PMID: 35839147.

[63] K. F. Mak, C. Lee, J. Hone, J. Shan, and T. F. Heinz, "Atomically thin MoS2: A new direct-gap semiconductor," *Physical Review Letters*, vol. 105, no. 13, pp. 2–5, 2010.

[64] A. Splendiani, L. Sun, Y. Zhang, T. Li, J. Kim, C. Y. Chim, G. Galli, and F. Wang, "Emerging photoluminescence in monolayer MoS2," *Nano Letters*, vol. 10, no. 4, pp. 1271–1275, 2010.

[65] T. Tomiki, Y. Ganaha, T. Shikenbaru, Y. Aiura, M. Yuri, S. Sato, H. Fukutani, Y. Aiura, H. Kato, T. Miyahar, J. Tamashi, and Y. Akira, "Anisotropic optical spectra of al203 single crystals in the vacuum ultraviolet region.ii.

spectra of optical constants," *Journal of the Physical Society of Japan*, vol. 62, no. 4, p. 1372 – 1387, 1993. Cited by: 35.

[66] E. D. Palik, *Handbook of optical constants of solids*, vol. 3. Academic press, 1998.

[67] A. B. Djurišić and E. Li, "Modeling the optical properties of sapphire (al2o3)," *Optics Communications*, vol. 157, no. 1, pp. 72–76, 1998.

[68] R. Kumar, V. Mishra, T. Dixit, P. K. Barman, P. K. Nayak, and M. S. Rao, "Observation of positive trions in $\alpha$-MoO3/MoS2 van der Waals heterostructures," *Nanoscale*, vol. 15, no. 29, pp. 12358–12365, 2023.

[69] S. Golovynskyi, O. I. Datsenko, D. Dong, Y. Lin, I. Irfan, B. Li, D. Lin, and J. Qu, "Trion Binding Energy Variation on Photoluminescence Excitation Energy and Power during Direct to Indirect Bandgap Crossover in Monolayer and Few-Layer MoS2," *Journal of Physical Chemistry C*, vol. 125, no. 32, pp. 17806–17819, 2021.

[70] D. Kaplan, K. Mills, J. Lee, S. Torrel, and V. Swaminathan, "Excitation intensity dependent photoluminescence of annealed two-dimensional MoS2 grown by chemical vapor deposition," *Journal of Applied Physics*, vol. 119, no. 21, 2016.

[71] X. Sun, Y. Zhu, H. Qin, B. Liu, Y. Tang, T. Lü, S. Rahman, T. Yildirim, and Y. Lu, "Enhanced interactions of interlayer excitons in free-standing heterobilayers," *Nature*, vol. 610, no. 7932, pp. 478–484, 2022.

[72] J. Shang, X. Shen, C. Cong, N. Peimyoo, B. Cao, M. Eginligil, and T. Yu, "Observation of excitonic fine structure in a 2D transition-metal dichalcogenide semiconductor," *ACS Nano*, vol. 9, no. 1, pp. 647–655, 2015.

[73] Y. You, X. X. Zhang, T. C. Berkelbach, M. S. Hybertsen, D. R. Reichman, and T. F. Heinz, "Observation of biexcitons in monolayer WSe 2," *Nature Physics*, vol. 11, no. 6, pp. 477–481, 2015.

[74] D. Kaplan, Y. Gong, K. Mills, V. Swaminathan, P. M. Ajayan, S. Shirodkar, and E. Kaxiras, "Excitation intensity dependence of photoluminescence from

monolayers of MoS2 and WS2/MoS2 heterostructures," *2D Materials*, vol. 3, no. 1, 2016.

[75] A. Steinhoff, J. H. Kim, F. Jahnke, M. Rösner, D. S. Kim, C. Lee, G. H. Han, M. S. Jeong, T. O. Wehling, and C. Gies, "Efficient Excitonic Photoluminescence in Direct and Indirect Band Gap Monolayer MoS2," *Nano Letters*, vol. 15, no. 10, pp. 6841–6847, 2015.

[76] B. Liu, A. Abbas, and C. Zhou, "Two-Dimensional Semiconductors: From Materials Preparation to Electronic Applications," *Advanced Electronic Materials*, vol. 3, no. 7, pp. 1–17, 2017.

[77] S. Ahmed and J. Yi, "Two-dimensional transition metal dichalcogenides and their charge carrier mobilities in field-effect transistors," *Nano-Micro Letters*, vol. 9, no. 4, pp. 1–23, 2017.

[78] V. Bender, T. Bucher, M. N. Mishuk, Y. Xie, I. Staude, F. Eilenberger, K. Busch, T. Pertsch, and B. N. Tugchin, "Spectroscopic Study of the Excitonic Structure in Monolayer MoS2 under Multivariate Physical and Chemical Stimuli," *Physica Status Solidi (A) Applications and Materials Science*, vol. 2300113, pp. 1–12, 2023.

[79] N. Saigal and S. Ghosh, "Evidence for two distinct defect related luminescence features in monolayer MoS2," *Applied Physics Letters*, vol. 109, no. 12, 2016.

[80] M. Buscema, G. A. Steele, H. S. van der Zant, and A. Castellanos-Gomez, "The effect of the substrate on the Raman and photoluminescence emission of single-layer MoS2," *Nano Research*, vol. 7, no. 4, pp. 561–571, 2014.

[81] M. Uda, A. Nakamura, T. Yamamoto, and Y. Fujimoto, "Work function of polycrystalline ag, au and al," *Journal of Electron Spectroscopy and Related Phenomena*, vol. 88-91, pp. 643–648, 1998. Proceedings of the Seventh International Conference on Electron Spectroscopy.

[82] A. H. Barajas-Aguilar, J. C. Irwin, A. M. Garay-Tapia, T. Schwarz, F. Paraguay Delgado, P. M. Brodersen, R. Prinja, N. Kherani, and S. J.

Jiménez Sandoval, "Crystalline structure, electronic and lattice-dynamics properties of NbTe2," *Scientific Reports*, vol. 8, no. 1, pp. 1–14, 2018.

[83] D. Cukjati, A. Prodan, N. Jug, H. J. Van Midden, S. W. Hla, H. Böhm, F. W. Boswell, and J. C. Bennett, "The instability of the NbTe2 surface structure," *Physica Status Solidi (A) Applied Research*, vol. 193, no. 2, pp. 246–250, 2002.

[84] X. Zhu, J. He, W. Liu, Y. Zheng, C. Sheng, Y. Luo, S. Li, R. Zhang, and J. Chu, "Revealing the modulation effects on the electronic band structures and exciton properties by stacking graphene/h-bn/mos2 schottky heterostructures," *ACS Applied Materials & Interfaces*, vol. 15, no. 1, pp. 2468–2478, 2023. PMID: 36583673.

[85] R. Yan, Q. Zhang, W. Li, I. Calizo, T. Shen, C. A. Richter, A. R. Hight-Walker, X. Liang, A. Seabaugh, D. Jena, H. Grace Xing, D. J. Gundlach, and N. V. Nguyen, "Determination of graphene work function and graphene-insulator- semiconductor band alignment by internal photoemission spectroscopy," *Applied Physics Letters*, vol. 101, no. 2, 2012.

[86] Y. Pan, S. Li, M. Ye, R. Quhe, Z. Song, Y. Wang, J. Zheng, F. Pan, W. Guo, J. Yang, and J. Lu, "Interfacial Properties of Monolayer MoSe2-Metal Contacts," *Journal of Physical Chemistry C*, vol. 120, no. 24, pp. 13063–13070, 2016.

[87] L. Huang, B. Li, M. Zhong, Z. Wei, and J. Li, "Tunable Schottky Barrier at MoSe2/Metal Interfaces with a Buffer Layer," *Journal of Physical Chemistry C*, vol. 121, no. 17, pp. 9305–9311, 2017.

[88] P. a. Bertrand, "Surface-phonon dispersion of ¡math display="inline"¿ ¡mrow¿ ¡msub¿ ¡mrow¿ ¡mi mathvariant="normal"¿MoS¡/mi¿ ¡/mrow¿ ¡mrow¿ ¡mn¿2¡/mn¿ ¡/mrow¿ ¡/msub¿ ¡/mrow¿ ¡/math¿," *Physical Review B*, vol. 44, no. 11, pp. 5745–5749, 1991.

[89] H. Li, Q. Zhang, C. C. R. Yap, B. K. Tay, T. H. T. Edwin, A. Olivier, and D. Baillargeat, "From bulk to monolayer MoS 2: Evolution of Raman

scattering," *Advanced Functional Materials*, vol. 22, no. 7, pp. 1385–1390, 2012.

[90] K. G. Zhou, F. Withers, Y. Cao, S. Hu, G. Yu, and C. Casiraghi, "Raman modes of MoS2 used as fingerprint of van der Waals interactions in 2-D crystal-based heterostructures," *ACS Nano*, vol. 8, no. 10, pp. 9914–9924, 2014.

[91] B. Chakraborty, H. S. Matte, A. K. Sood, and C. N. Rao, "Layer-dependent resonant Raman scattering of a few layer MoS2," *Journal of Raman Spectroscopy*, vol. 44, no. 1, pp. 92–96, 2013.

[92] K. Zhang, Z. Y. Cao, and X. J. Chen, "Effects of charge-density-wave phase transition on electrical transport and Raman spectra in 2 H -tantalum disulfide," *Applied Physics Letters*, vol. 114, no. 14, 2019.

[93] K. Kang, S. Xie, L. Huang, Y. Han, P. Y. Huang, K. F. Mak, C. J. Kim, D. Muller, and J. Park, "High-mobility three-atom-thick semiconducting films with wafer-scale homogeneity," *Nature*, vol. 520, no. 7549, pp. 656–660, 2015.

[94] B. Tang, Z. G. Yu, L. Huang, J. Chai, S. L. Wong, J. Deng, W. Yang, H. Gong, S. Wang, K. W. Ang, Y. W. Zhang, and D. Chi, "Direct n- to p-Type Channel Conversion in Monolayer/Few-Layer WS2 Field-Effect Transistors by Atomic Nitrogen Treatment," *ACS Nano*, vol. 12, no. 3, pp. 2506–2513, 2018.

[95] M. Velický, G. E. Donnelly, W. R. Hendren, S. McFarland, D. Scullion, W. J. DeBenedetti, G. C. Correa, Y. Han, A. J. Wain, M. A. Hines, D. A. Muller, K. S. Novoselov, H. D. Abruńa, R. M. Bowman, E. J. Santos, and F. Huang, "Mechanism of gold-assisted exfoliation of centimeter-sized transition-metal dichalcogenide monolayers," *ACS Nano*, vol. 12, no. 10, pp. 10463–10472, 2018.

[96] J. D. Andrade, *X-ray Photoelectron Spectroscopy (XPS)*, pp. 105–195. Boston, MA: Springer US, 1985.

[97] R. Scarfiello, E. Mazzotta, D. Altamura, C. Nobile, R. Mastria, S. Rella, C. Giannini, P. D. Cozzoli, A. Rizzo, and C. Malitesta, "An insight into chemistry and structure of colloidal 2d-ws2 nanoflakes: Combined xps and xrd study," *Nanomaterials*, vol. 11, no. 8, 2021.

[98] A. P. Shpak, A. M. Korduban, L. M. Kulikov, T. V. Kryshchuk, N. B. Konig, and V. O. Kandyba, "XPS studies of the surface of nanocrystalline tungsten disulfide," *Journal of Electron Spectroscopy and Related Phenomena*, vol. 181, no. 2-3, pp. 234–238, 2010.

# Appendix A

# Code